# RESONANT OPTICAL NANOANTENNAS AND APPLICATIONS

A THESIS

SUBMITTED TO THE PROGRAM OF MATERIAL SCIENCE AND

NANOTECHNOLOGY

AND THE INSTITUTE OF ENGINEERING AND SCIENCES

OF BILKENT UNIVERSITY

IN PARTIAL FULFILLMENT OF THE REQUIREMENTS

FOR THE DEGREE OF

MASTER OF SCIENCE

By

Murat Celal KILINÇ

August 2010

I certify that I have read this thesis and that in my opinion it is fully adequate, in scope and in quality, as a thesis for the degree of Master of Science.

Assist Prof. Dr. Mehmet Bayındır (Supervisor)

I certify that I have read this thesis and that in my opinion it is fully adequate, in scope and in quality, as a thesis for the degree of Master of Science.

Assist Prof. Dr. Ali Kemal Okyay

I certify that I have read this thesis and that in my opinion it is fully adequate, in scope and in quality, as a thesis for the degree of Master of Science.

Assist Prof. Dr. Selçuk Aktürk

Approved for the Institute of Engineering and Sciences:

Prof. Dr. Levent Onural
Director of Institute of Engineering and Sciences

# ABSTRACT

# RESONANT OPTICAL NANOANTENNAS AND APPLICATIONS

Murat Celal KILINÇ

M.S. in Material Science and Nanotechnology

Supervisor: Assist Prof. Dr. Mehmet Bayındır

August 2010

Being one of the fundamentals of electrical engineering, an antenna is a metallic shape structured to transmit or receive electromagnetic waves. Thanks to the recent advances in nano fabrication and nano imaging, metallic structures can be defined with sizes smaller to that of visible light, wavelengths of several nanometers. This opens up the possibility of the engineering of antennas working at optical wavelengths. Nanoantennas could be thought of optical wavelength equivalent of common antennas. Today physics, chemistry, material science and biology use optical nanoantennas to control light waves. Optical nanoantennas are tailored for many technological applications that include generation, manipulation and detection of light. The near field enhancement of resonant optical nanoantennas at specific wavelengths is their most promising advantage that attracts technological applications. In this thesis, we study the resonance characteristics of optical nanoantennas and investigate the governing factors by numerical calculations. We also evaluate radiated electric field from the resonating nanoantenna. Finally, we employ the resonant near field enhancement in optical

nonlinear generation. The fabrication of nanoantennas with FIB milling is also explored.

# ÖZET

## OPTİK DALGA BOYLARINDA ÇALIŞAN, REZONE EDEN NANOANTENLER VE UYGULAMALARI

Murat Celal KILINÇ
Malzeme Bilimi ve Nanoteknoloji Bölümü Yüksek Lisans
Tez Yöneticisi: Yar. Doç. Dr. Mehmet Bayındır
Ağustos 2010

Elektrik mühendisliğinin temel yapıtaşlarından olan antenler elektromanyetik dalgaları yaymak ve almak için tasarlanmış metal şekillerdir. Nano fabrikasyon ve nano boyutta görüntüleme tekniklerinin gelişmesi ile birlikte metal şekillerin görünür ışığın dalgoboyundan küçük boyutlarda, nano boyutlarda, dahi fabrike edilmesi mümkün hale gelmiştir. Nano boyutlu metal şekiller sayesinde optik dalga boylarında çalışan antenlerin mühendisliğinin önü açılmıştır. Nano antenler radyo antenlerinin optik dalga boylarında çalışan eşdeğeri sayılabilir. Bugün, fizik, kimya, malzeme bilimi ve biyoloji nanoantenleri ışık dalgalarını kontrol etmek için kullanmaya başlamıştır. Nanoantenler ışığın üretiminin, manipülasyonunun ve algılanmasının yer aldığı teknolojik uygulamalar için düzenlenmektedirler. Optik nanoantenlerin rezone ettikleri dalga boyları için, yüzeylerinde ve yüzeylerine yakın yerlerde, dikkat çeken elektrik alan artışı gözlenmektedir. Bu elektrik alan artışı teknolojik uygulamalar açısından oldukça önemlidir. Bu tezde nümerik hesaplamalar yoluyla optik nanoantenlerin rezonans

karakterleri ve rezonanslarını etkileyen etkenler çalışılmıştır. Bunun yanında, rezone eden nanoantenlerin radyasyon karakterleri incelenmiştir. Son olarak, rezone eden nanoantenlerin yakınındaki yüksek elektrik alan lineer olmayan optik uygulamalar için kullanılmıştır. Odaklanmış iyon demeti yoluyla nanoantenlerin fabrikasyonlarının sonuçları da sunulmuştur.

*Anahtar Kelimeler:* Nanoanten, Plazmonik, Lineer Olmayan Optik, Çalkojen Cam

# ACKNOWLEDGMENTS

Firstly, I would like to thank to my thesis advisor Assist Prof. Mehmet Bayındır for his supervision during this study at UNAM. UNAM is mainly remembered with a couple of energetic people: Assist Prof. Aykutlu Dana, Assist Prof. Mehmet Bayındır and Prof. Salim Çıracı. Their effort for the establishment of a national center for excellence in nanotechnology research is a devotion for state of the art science and technology leap in Turkey.

Secondly, I would like to thank to Dr. Mecit Yaman for his scientific and personal wisdom. I am delighted to be one of those he enlightened.

Thirdly, I would like to thank to TUBITAK for financial support through 2228 coded scholarship.

Finally, I would like to thank to friends at UNAM: Kemal Gürel, Mert Vural, Adem Yildirim, Koray Mızrak, Burkan Kaplan, Neslihan Arslanbaba, Özlem Şenlik, Yavuz Nuri Ertaş, Hasan Esat Kondakçı, Özlem Köylü, Erol Özgür, Ekin Özgür, Duygu Akbulut, Hülya Budunoğlu, Dr. Hakan Deniz, Dr. Abdullah Tülek, Can Koral and Ahmet Ünal.

# Contents

# List of Figures

# List of Tables

Dedicated to my family

# Chapter 1

# INTRODUCTION

In the parlor of electrical engineering, an antenna is a metallic rod, wire or other shape structured to transmit or receive electromagnetic waves [10]. Recent advances in nano fabrication, electron microscopy imaging and near field microscopy allowed metallic structures to be defined and characterized with sizes comparable or smaller to that of visible light, wavelengths of several hundred nanometers, opened up the possibility of optical radio engineering: Nanoantennas are optical wavelength equivalent of common antennas [11]. Today, a wide spectrum of scientists, ranging from physicists, chemists and materials scientists to biologists use optical antennas to control light waves. Optical nanoantennas are tailored for many technological applications that include generation, manipulation and detection of light. For instance, nanooptical microscopy, single molecule absorption spectroscopy, extreme ultraviolet light generation, infrared photodetection, solar energy conversion and even photothermal tumor therapy exploit the benefits of optical nanoantennas [5–8,12–14]. The near field enhancement of optical nanoantennas at specific wavelengths is their most promising advantage that attracts those technologies.

In this thesis, we study the resonance characteristics of optical nanoantennas and investigate the governing factors. Furthermore, we evaluate the nanoantenna radiation at resonance. Finally, we employ the resonant near field enhancement in optical nonlinear generation. The fabrication of nanoantennas with FIB milling is also explored.

Our contributions can be summarized as follows:

- We show that resonance characteristics of optical nanoantennas for a specific incident wavelength is governed by substrate, antenna length along the polarization direction of the incident electric field and the antenna shape.

- We also show that we can account for the $E_x{}^2$, $E_y{}^2$ and $E_z{}^2$ components of nanoantenna radiaton at resonance by taking into account the electron acceleration due to specific $E$ and $B$ components of the incident optical field.

- Furthermore, we also employ the near field of the resonant optical nanoantenna for lowering the required large incident electric field for optical nonlinear generations.

- Finally, we show that the fabrication of nanoantennas with FIB milling is fast yet substrate dependent.

In Chapter 2, we first provide theoretical preliminaries that are necessary for the development of the thesis work. Chapter first addresses the counterpart concepts in the field of radio antenna engineering. Then it reviews the electromagnetics of metals for understanding the optical phenomena of metallic nano structures and finally, the chapter presents the optical antenna characteristics and applications in the literature. In Chapter 3, we first compare and contrast the near field response of various nanoantennas for a specific wavelength incident optical radiation. Then, we describe the interaction of the optical field, resonant

optical nanoantenna and the substrate. Finally, we concentrate on the nonlinear optical interaction of the resonant nanoantenna near field with a nonlinear (optical) substrate. Next, Chapter 4 presents fabrication of gold nanoantennas with FIB milling. We conclude and list future research areas in the Chapter 5.

# Chapter 2

# BACKGROUND

In order to survey fundamental concepts pertinent to nano optical transceivers, in this chapter, we start by reviewing counterpart concepts in the well established field of radio antenna engineering followed by a brief discussion of the electromagnetics of metals which is also essential in understanding optical phenomena of metallic nano structures. Finally, we review the optical antenna research literature, including both the nanoantenna characteristics and promising technological applications.

## 2.1 Antenna Fundamentals

An antenna is a device for receiving or radiating electromagnetic energy [10]. When incoming radiation causes a dynamic current distribution to occur on an antenna, it is said to be a receiver, when an externally driven dynamic current distribution on the antenna causes radiation it is said to be a transmitter. Most antennas are reciprocal meaning that they both receive or transmit. Moreover, some antennas focus incoming electromagnetic waves, receiving and transmitting simultaneously.

When an electric charge accelerates it radiates energy in the form of electromagnetic waves [15]. Thus, Hecht defines the condition for radiation from an antenna as acceleration or deceleration of free charges on the antenna. In other words time varying current on the antenna provides radiation into the surrounding medium. The resulting radiation field is transverse to charge velocity. A source with a particular electronic circuitry generates time varying current and a particular guiding device is responsible for appropriate current transport from source to antenna.

Antennas are generally described with characteristic performance parameters: radiation pattern, radiation power density, radiation intensity, beamwidth, directivity, gain, bandwidth, polarization, input impedance [10].

The radiation pattern represents directional variation of performance parameters in a transmitter antenna. A trace of electric or magnetic field at a constant distance from the antenna is the amplitude field pattern whereas a similar trace of electric or magnetic power density is the amplitude power pattern. The radiation pattern is usually has bulging portions called lobes. Radiation lobes are high intensity directions surrounded by weaker radiation directions. The major lobe includes the direction of maximum radiation which is the desired radiation direction. Any lobe other than the major lobe is a minor lobe. The radiation pattern of an antenna changes depending on the distance from the antenna. This change in field pattern results that the space surrounding the antenna divided into three field regions: reactive near field, radiating near field (Fresnel) and far field (Fraunhofer). The reactive near field region starts from the radiating surface of the antenna and terminates about a wavelength of the transceived wave. In this region the energy decays very rapidly with distance from the radiating surface (energy decays with the third and fourth power of the distance) and the field pattern is nearly homogeneous although there are localized energy fluctuations. The radiating near field region is between reactive near field and far field
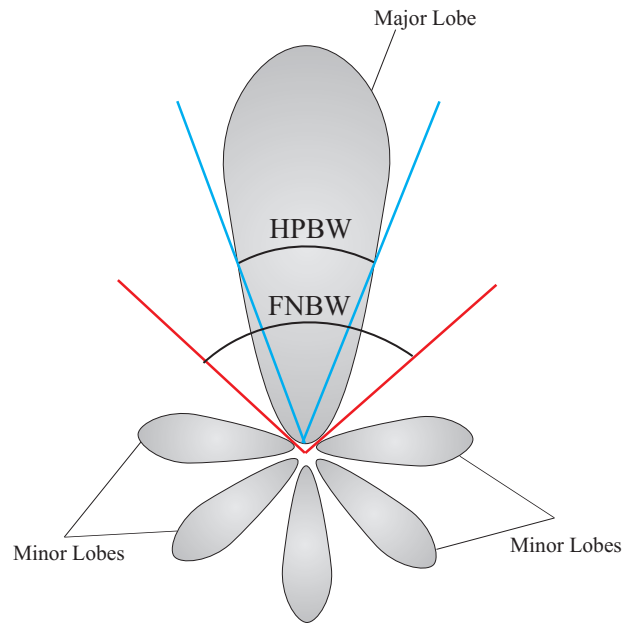
Figure 2.1: A typical radiation pattern of an antenna.

regions. In this radiation field region the field pattern depends on the distance from the antenna and it begins to form lobes. If the antenna dimensions are very small compared to wavelength, the radiating near field region diminishes. The boundary between radiating near field and far field regions is defined as the distance $2D^2/\lambda$ where $D$ is the largest dimension of the antenna. Beyond this distance is the far field region where the field pattern is well formed and does not vary with distance from the antenna. Here the energy decays with the square of distance from the radiating surface.

The radiation power density $W$ of an antenna is the time average Poynting vector whereas the radiation intensity $U$ is the directional power radiated from the antenna per unit solid angle. Radiation intensity $U$ is a far field parameter and obtained by multiplying the radiation power density by distance square, $U = r^2 W$.

The beamwidth of an antenna is is a quantity associated with the radiation pattern. The angular distance between two identical points on opposite sides of the field pattern is defined to be the beamwidth. As a convention, half power

beamwidth (HPBW) is defined to be the angle between two sides of the field pattern where the radiation intensity is half of its peak value in the direction of maximum antenna radiation. Furthermore, first null beamwidth (FNBW) is the angle between first nulls of the field pattern. Figure 2.1 demonstrates radiation pattern, lobe and beamwidth concepts.

The directivity $D$ of an antenna is the ratio of the radiation intensity $U$ in a particular direction to the radiation intensity averaged over all directions $U_0 = P_{rad}/4\pi$. If a particular direction is not specified, it is taken to be the the direction of maximum radiation.

$$D = \frac{U}{U_0} = \frac{U}{P_{rad}/4\pi} \tag{2.1}$$

The gain $G$ of an antenna is the ratio of the radiation intensity $U$ in a particular direction to the antenna input power intensity averaged over all directions. Again, if a particular direction is not specified, it is taken to be the the direction of maximum radiation. A constant called radiation efficiency $e_{cd}$ is defined in order to relate input and radiated power intensities $P_{rad} = e_{cd}P_{in}$. Radiation efficiency embodies conduction and dielectric losses of the antenna. It does not include the mismatch loss between source and guiding device couple and the antenna. Thus directivity and gain can be related.

$$G = \frac{U}{P_{in}/4\pi} = e_{cd}D \tag{2.2}$$

The bandwidth of an antenna is the range of frequencies where the antenna performance parameters individually have an acceptable value compared to those at the antenna center frequency.

The polarization of an antenna is the electromagnetic polarization of the radiated wave in a particular direction. If a particular direction is not specified,

it is taken to be the the direction of maximum gain. Polarization is categorized as linear, circular and elliptical. If the electric or magnetic field vector of the radiated wave at a point is always directed along a line at every instant of time, the field is said to be linearly polarized.

The input impedance $Z_A$ of an antenna is the impedance presented by the antenna at its terminals, $Z_A = R_A + jX_A$. Here $R_A$ is the input resistance and embodies power dissipations due to radiative and ohmic losses. $X_A$ is the input reactance and represents reactive power losses.

As a consequence of reciprocity theorem, radiation pattern, radiation power density, radiation intensity, beamwidth, directivity, gain, bandwidth, polarization and input impedance of an antenna are identical during transmission and reception.

Common radio antenna, half wavelength linear dipole ($l = \lambda/2$) is a standing wave antenna because the dynamic current distribution on the antenna has a standing wave pattern. For $l = \lambda/2$ the input reactance $X_A$ of the antenna vanishes and the antenna is said to be resonant in analogy with a resonant RLC circuit [16]. At resonance the input impedance of the antenna is purely resistive and reactive losses due to $X_A$ are neglected.

## 2.2  Electromagnetics of Metals

Maxwell's equations are sufficient to describe the interaction of metals with electromagnetic fields [17]. Even if the metal is nanometer sized, quantum mechanics is not required. This is a result of the high density of free electrons in metals. High density of free electrons ensures very close electron energy levels and even nanometer sized metals can be explored classically.

Metals reflect electromagnetic waves for frequencies up to about visible. In this frequency regime metals are highly conductive and only negligible electromagnetic wave penetrates into the metal. At higher frequencies dielectricity of metal becomes noticeable and wave penetration increases. This dispersive character of metals is described with the complex dielectric function $\varepsilon(\omega)$ since all electromagnetic phenomena depends on $\varepsilon(\omega)$. Furthermore, the underlying physics behind this dispersive character is the phase difference between electromagnetic wave and free electron oscillation which arises due to the particular electron relaxation time $\tau$ of the metal.

Plasma model is a valid approximation over a wide frequency range for explaining dispersive characteristics of metals [17]. In this model free electron gas of number density $n$ is assumed to be moving against fixed background of positive ion cores. The electron motion is a damped oscillation due to collisions with collision frequency $\gamma$ which is due to the particular relaxation time of the metal, $\gamma = 1/\tau$. $\tau$ is in the order of $10^{-14}$ s at room temperature, corresponding to $\gamma = 100$ THz. A simple representation of metallic band structure is also incorporated into the effective electron mass $m$. Thus plasma model equation of motion for an electron subjected to an external time harmonic electric field $E$ is

$$m\ddot{x} + m\gamma\dot{x} = -qE(t), \qquad (2.3)$$

where $x$ is the electron displacement and $q$ is the electron charge. For $E(t) = E_0 e^{-i\omega t}$ driving field, a particular solution to the equation of motion for an electron is

$$x(t) = \frac{q}{m(\omega^2 + i\gamma\omega)}E(t). \qquad (2.4)$$

9

The complex amplitude of $x(t)$ absorbs the phase difference between driving field and electron displacement. Thus the macroscopic polarization $P = -nqx$ becomes

$$P = -\frac{nq^2}{m(\omega^2 + i\gamma\omega)}E.$$ (2.5)

Embedding polarization $P$ to the electric flux, $D = \epsilon_0\epsilon E = \epsilon_0 E + P$ yields

$$D = \epsilon_0\left(1 - \frac{\omega_p{}^2}{\omega^2 + i\gamma\omega}\right)E,$$ (2.6)

where $\omega_p{}^2 = \frac{nq^2}{\epsilon_0 m}$ is the plasma frequency of the particular metal. Hence the complex dielectric function of a metal $\epsilon(\omega) = \epsilon_1(\omega) + j\epsilon_2(\omega)$ is obtained where

$$\epsilon_1(\omega) = 1 - \frac{\omega_p{}^2\tau^2}{1 + \omega^2\tau^2},$$ (2.7)

$$\epsilon_2(\omega) = \frac{\omega_p{}^2\tau}{\omega(1 + \omega^2\tau^2)}.$$ (2.8)

The plasma frequency $\omega_p/2\pi$ and the corresponding plasma wavelength $\lambda_p$ of common metals are 3570 THz / 85 nm for Al, 1914 THz / 156 nm for Cu, 2175 THz / 138 nm for Ag and 2175 THz / 138 nm for Au [18]. The collision frequency $\gamma$ of common metals are 175 THz for Al [19], 14 THz for Ag [20] and 6 THz for Au [21].

At frequencies $\omega < \omega_p$ and $\omega \ll \tau^{-1}$, metals are so conductive that only negligible electromagnetic wave penetrates. Here $\epsilon_2 \gg \epsilon_1$ and $\epsilon_1$ is negative. Thus, the real and the imaginary parts of the complex refractive index $\tilde{n} = \sqrt{\epsilon} = n(\omega) + j\kappa(\omega)$ becomes comparable in magnitude with

$$n \approx \kappa = \sqrt{\frac{\epsilon_2}{2}} = \sqrt{\frac{\tau \omega_p{}^2}{2\omega}}. \tag{2.9}$$

The absorption coefficient $\alpha$ in Beer's law describes how the intensity of the electromagnetic wave propagating into a medium attenuates. Since $\alpha = \frac{2\kappa\omega}{c}$, the absorption coefficient for $\omega \ll \tau^{-1}$ becomes

$$\alpha = \frac{\sqrt{2\tau\omega_p{}^2\omega}}{c} \tag{2.10}$$

The intensity of the electromagnetic wave penetrating into the metal decays with $e^{-z/\delta}$, where $\delta = 2/\alpha$ is defined as the skin depth of the particular metal.

At frequencies $\omega < \omega_p$ and $\omega \gg \tau^{-1}$, $\epsilon(\omega)$ is practically real, $\epsilon_2(\omega) \approx 0$, and

$$\epsilon(\omega) = 1 - \frac{\omega_p{}^2}{\omega^2}. \tag{2.11}$$

However, in this frequency band interband transitions cause metals behave differently. At higher frequencies $\omega > \omega_p$, the dielectricity of metal becomes so high that this is described by an extra dielectric constant, $\epsilon_\infty$ ($1 \leq \epsilon_\infty \leq 10$)

$$\epsilon(\omega) = \epsilon_\infty - \frac{\omega_p{}^2}{\omega^2 + i\gamma\omega} \tag{2.12}$$

Figure 2.2 shows real $\epsilon_1(\omega/2\pi)$ and imaginary $\epsilon_2(\omega/2\pi)$ parts of the complex dielectric function of gold. The material data is taken from Palik's Handbook of Optical Constants and used by Lumerical FDTD for numerical calculations.
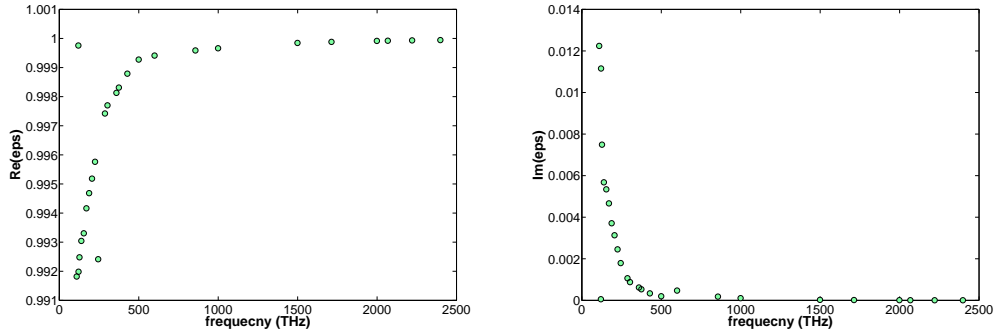
Figure 2.2: Real $\epsilon_1(\omega/2\pi)$ and imaginary $\epsilon_2(\omega/2\pi)$ parts of the dielectric function of gold.

## 2.3 Resonant Optical Nanoantennas and Applications

Concentrating light in the nanometer scale, using subwavelength sized metallic structures, has recently developed into a new branch of photonics called plasmonics, or more descriptively nanophotonics which eponymously announces the overcoming of the diffraction limit. Plasmonics is a resonant phenomenon that is based on the interaction of light with conduction electrons in nanostructured metals [17]. It has the promise of merging photonic capacities with that of reduced size integrated electronics. [22].

Nanoantennas enable optimum conversion of propagating light into subwavelength localized optical fields [1, 2, 4, 23–27]. Concentrating light leads to electric field enhancement [28]. Thus optical antennas allow manipulating light matter interaction in the reactive near field of the nanoantennas rendering them indispensable in many technological applications such as fluorescence microscopy, absorption spectroscopy, control of single molecule emission, extreme ultraviolet light generation, infrared photodetection, solar energy conversion and photothermal tumor therapy [5–8, 12–14]. Hence nanoantennas are expected to find many applications in greatly improving the efficiency of the optoelectronic devices [23].
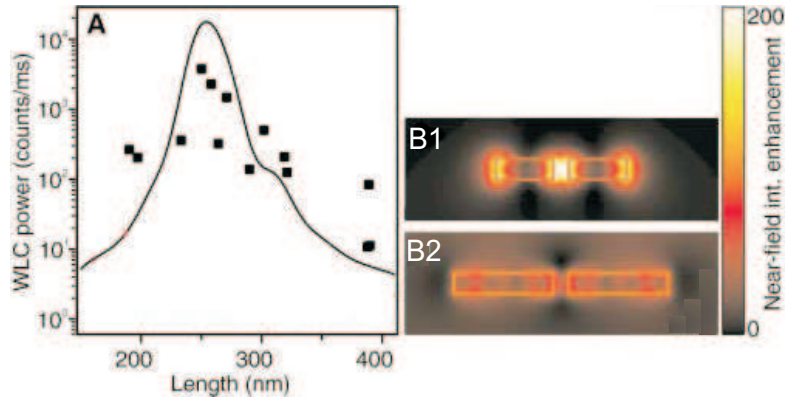
Figure 2.3: (A) Variation of WLSC power with antenna length, filled squares. Solid curve represents calculated near field intensity response without a y-axis. (B1 to B2) Calculated spatial near field on 10 nm above the dipole nanoantennas at $\lambda = 830$ nm. (B1) At resonance (B2) Out of resonance [1].

Incident light induces oscillations of the metal's free electrons. Thus upon illumination several harmonic current waves with different amplitudes and phases are created within the antenna skin depth. At resonance interference of those current waves results in a standing wave. In other words, at resonance a collective charge oscillation is created on the antenna which produces the enhanced reactive near field. The enhancement of the field is determined by the resonance properties. Unlike radio antennas, the reactive near field of nanoantennas are of importance because incident light is said to be confined in the reactive near field of the nanoantenna. Since current electronics is speed limited, the resulting current wave on the nanoantenna cannot be manipulated by an electronic circuitry.

The pioneering work of Mühlschlegel *et al* in 2005 introduces the solid frame of optical antenna research [1]. They show that resonance depends on the antenna length and the polarization of the incident light. This is proved with numerical calculations and experimental demonstration. Gold dipole antennas fabricated on glass substrate are illuminated with picosecond linearly polarized laser pulses at $\lambda = 830$ nm. The enhanced near field of the resonant nanoantennas are used to boost nonlinear phenomena. The antennas lying along the polarization direction

13
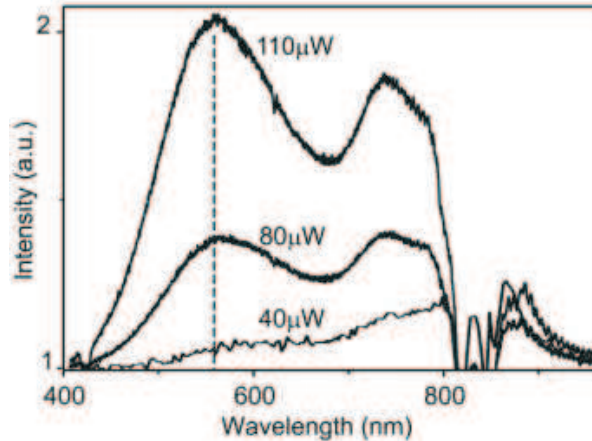
Figure 2.4: Measured WLSC spectra of a resonant dipole nanoantenna for three different average power levels of the pulsed Ti:sapphire laser, excitation wavelength $\lambda = 830$ nm [1].

and of particular length generate white light supercontinuum (WLSC) radiation. WLSC generation is due to the third order optical nonlinearity of glass substrate and the optical power coming from the laser and sufficiently enhanced by the nanoantenna. Figure 2.3A shows WLSC power and near field enhancement for different dipole lengths. Figure 2.4 shows WLSC spectra coming from a resonant dipole, only short wavelength wing of the spectra is considered though.

Ghenuche *et al* illustrate the modes and the modal field distributions of resonant nanoantennas [2]. In analogy with the standing current wave modes of the linear dipole radio antenna ($l = n\lambda/2$, n being an integer) [10], the modes of the nanoantenna are associated with the resonances using the relation between the antenna length $L$ and the effective wavelength $\lambda_eff$: $L = (n + 1/2)\lambda_eff$ (n being an integer). As shown in figure 2.5 additional weaker field modulations along the sides of the nanoantennas address higher order resonant modes, namely $3\lambda_eff/2$ and $5\lambda_eff/2$ resonances. The $3\lambda_eff/2$ resonance of the 500 nm long stripe antenna occurs at $\lambda = 710$ nm (n=1 with $\lambda_eff = 333$ nm). However, the same mode of the dipole consisting of 500 nm long stripes with 40 nm gap shifts to $\lambda = 730$ nm. That $5\lambda_eff/2$ mode of the 1 $\mu m$ long stripe appears at $\lambda = 760$ nm (n=2 with $\lambda_eff = 400$ nm). Furthermore, authors explain the resonance

14
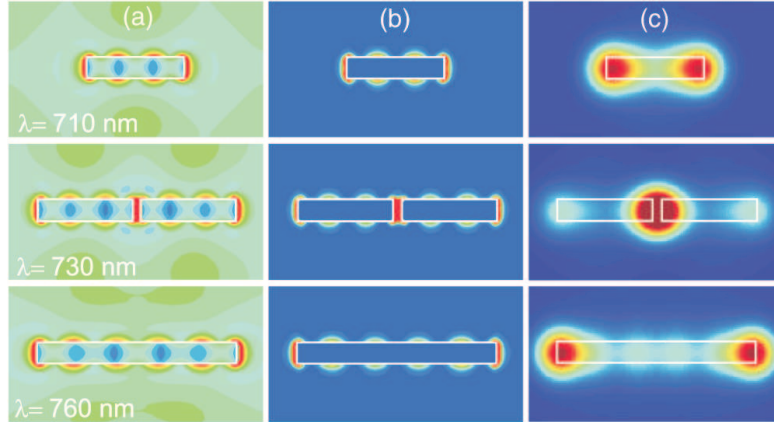
Figure 2.5: (a) Calculated spatial near field $| E |$ and (b) $| E |^4$ of the three types of antennas at their respective resonance wavelength. (c) is obtained by convoluting the $| E |^4$ maps with a 200 nm waist 2D Gaussian profile and integrating over the third dimension. [2].
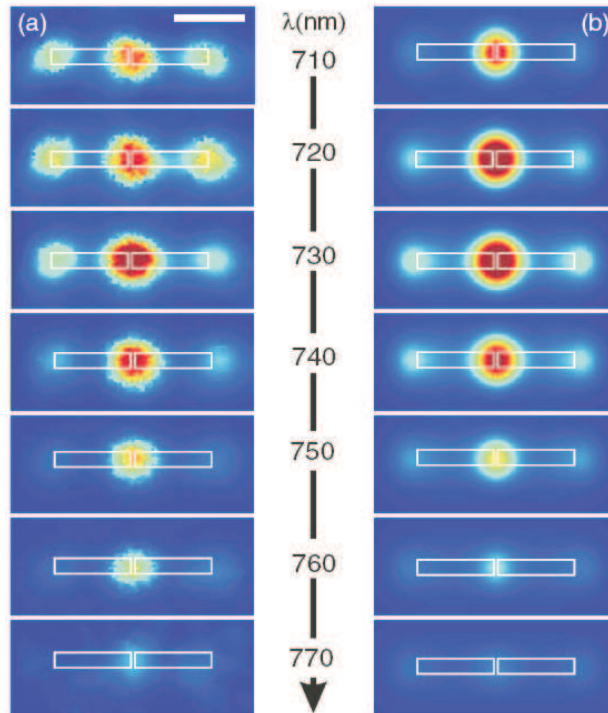


Figure 2.6: (a) Luminescence map of the dipole nanoantenna for different wavelengths. (b) Calculated convoluted $| E |^4$ distribution over a dipole nanoantenna [2].
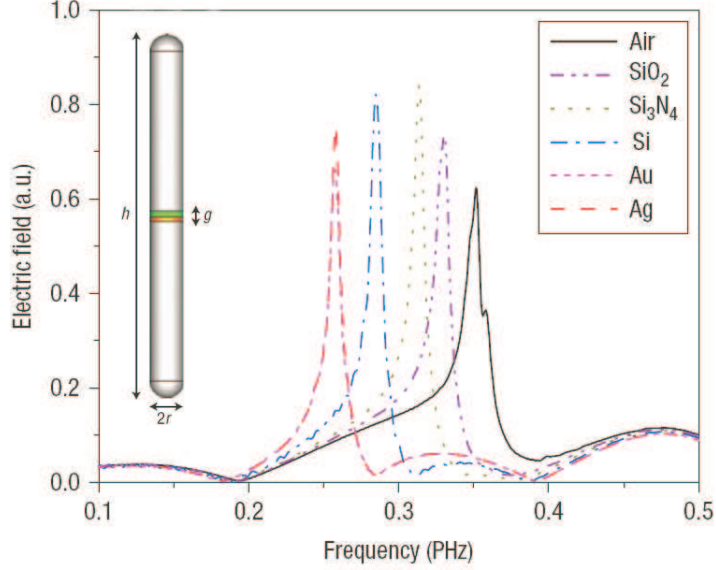
Figure 2.7: Far-field scattered electric-field amplitude calculated on the side of the dipole nanoantenna. The scattering resonance shifts with different materials filling the gap. $\varepsilon_{SiO_2} = 2.36\varepsilon_0$, $\varepsilon_{Si_3N_4} = 4.01\varepsilon_0$, $\varepsilon_{Si} = 13.35\varepsilon_0$ [3].

bandwidth of the optical antennas. Gold dipole nanoantenna fabricated on glass substrate is illuminated with femtosecond laser pulses to promote nonlinear effects. The wavelength is scanned from 710 to 770 nm in steps of 10 nm. Since the measured luminescence is the signature of the resonant field enhancement, bandwidth of the dipole has been determined. The results are compared with numerical calculations as shown in Figure 2.6.

In addition to antenna length, nanoantenna resonance can be tuned by a mechanism similar to impedance matching [3]. Alu and Engheta, by means of numerical modelling, show that the response of dipole nanoantennas can be tailored dramatically by changing the material inside the dipole gap. Filling a few nanometer cube volume of the gap with materials of higher permittivities causes the optical dipole resonance to shift towards higher wavelengths. Figure 2.7 represents the tuning phenomena for a silver nanoantenna, $h = 110$ nm, $r = 5$ nm, $g = 3$ nm. However, the near field response is not given instead it is converted to far field. More complex tuning is achieved by filling the gap with parallel or series combinations of different permittivities as shown in figure 2.8.

16
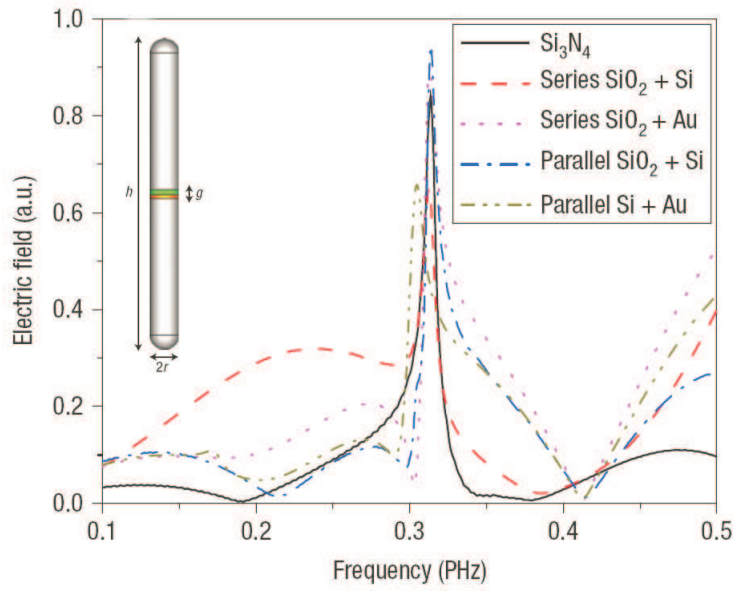
Figure 2.8: Far-field scattered electric-field amplitude calculated on the side of the dipole nanoantenna. The scattering resonance shifts with different materials filling the gap. In the series combination of silicon and $SiO_2$ the thicknesses of the nanodisks are $t_{Si} = t_{SiO_2} = 1.5$ nm; in the series combination of $SiO_2$ and gold, $t_{SiO_2} = 1.83$ nm and $t_{Au} = 1.17$ nm; in the parallel combination of silicon and SiO2, $r_{in} = 4.61$ nm; in the parallel combination of silicon and gold, $r_{in} = 4.56$ nm [3].
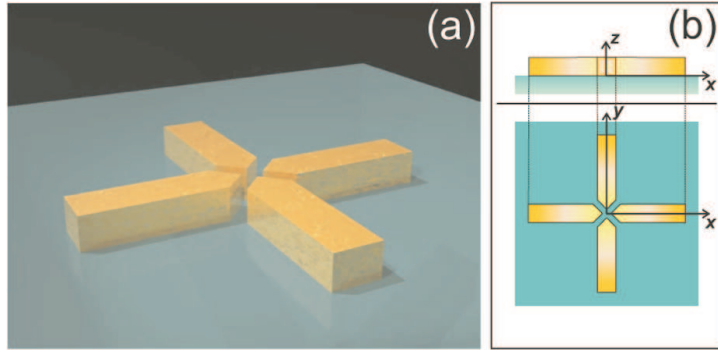
Figure 2.9: (a) The cross resonant optical antenna structure. Gold nanoantennas on glass substrate have a cross section of $20nm \times 20nm$ and a tip to tip distance of 10 nm. (b) The reference frame used. [4].
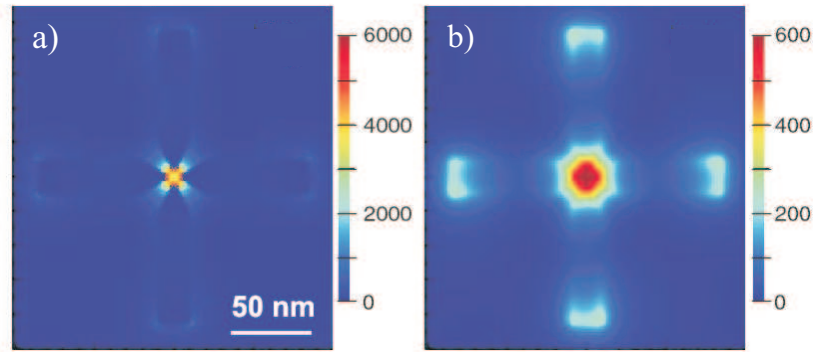


Figure 2.10: Calculated spatial near field (a) In a plane at midheight of the structure, $z = 10$ nm (b) 5 nm above the upper antenna surface, $z = 25$ nm [4].

Optical antennas should lie along the polarization direction of the propagating electromagnetic wave in order to resonate. However, a symmetrical geometric design can be used to eliminate this limitation [4]. Numerical calculations demonstrate that a structure consisting of two perpendicular dipole nanoantennas with a common feed gap is capable of resonating with any arbitrary polarization state carried of a propagating electromagnetic wave. Figure 2.9 shows this symmetrical structure. The cross resonant nanoantenna is illuminated with a circularly polarized light at $\lambda = 800$ nm, figure 2.10 shows the obtained near field proving that the cross resonant nanoantenna can be used as a local and enhanced source of circularly polarized photons.
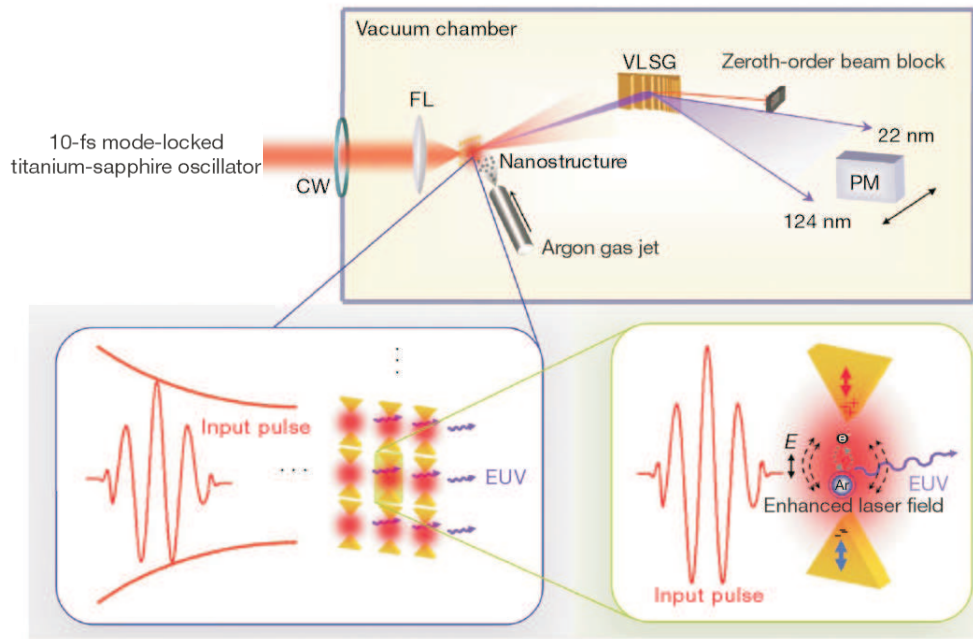
Figure 2.11: System for EUV generation. Ar, argon atom; CW, chamber window; FL, focusing lens; VLSG, varied-line-spacing grating; PM, photon multiplier. The laser is at $\lambda = 800$ nm with 100 kW peak power and 1.3 nJ pulse energy, producing intensity of $10^{11}$ W$cm^{-2}$ when well focused. [5].
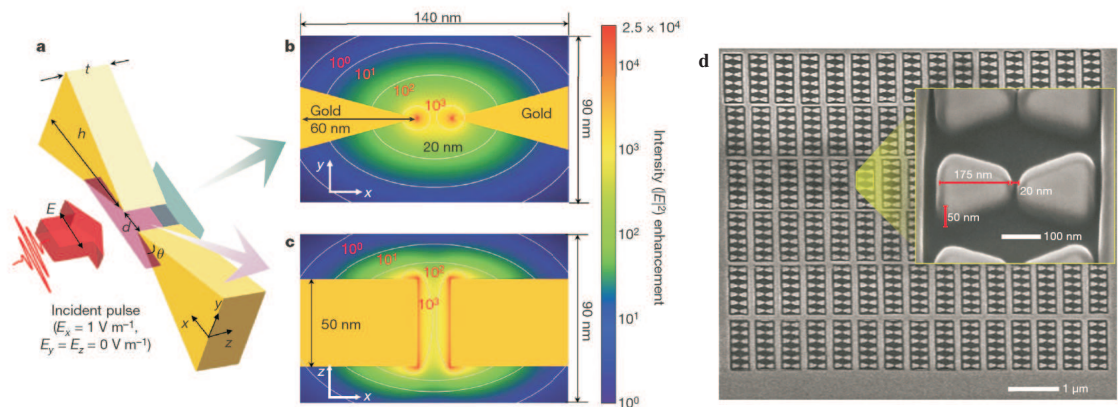


Figure 2.12: (a) The bow-tie antenna structure and the reference frame used. $h = 175$ nm, $d = 20$ nm, $t = 50$ nm, $\theta = 30°$ (b) to (c) Calculated spatial near field of the resonant optical bow-tie (d) SEM image of the nanostructure used. Antennas are arranged as an array of area $10\mu m \times 10\mu m$. Edge lines are seen blurred due to high magnification. [5].
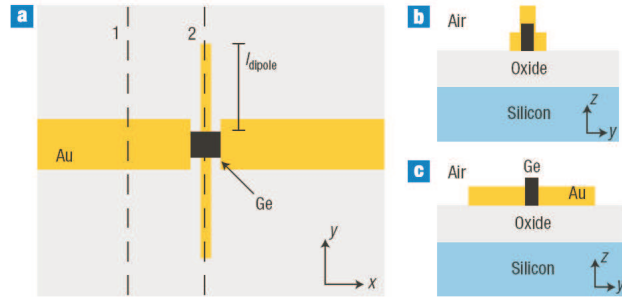
Figure 2.13: Open sleeve dipole structure. (a) Top view, dipole antenna is oriented in the y direction and two line electrodes (sleeves) are oriented in the x direction. (b) Cross section through line 1. (c) Cross section through line 2. [6].

The local field enhancement of resonant nanoantennas has the potential to reduce the required high optical intensities of some applications. One such application is the high harmonic generation by focusing a femtosecond laser onto a gas and producing coherent extreme ultraviolet (EUV) light. However, the process requires high pulse intensities, greater than $10^{13}$ $Wcm^{-2}$, which is normally achieved via complex optical amplification techniques. Kim *et al* exploit the near field enhancement of bow-tie nanoantennas to obtain EUV light [5]. Their system is shown in figure 2.11. Gold bow-tie nanoantenna array fabricated on sapphire substrate is illuminated with femtosecond laser pulses of intensity $10^{11}$ $Wcm^{-2}$ while facing the argon gas jet. As seen in figure 2.12, resonant bow-tie increases incident intensity by two orders of magnitude; hence, the threshold required to generate high harmonics is easily obtained. As a result, constructive interference of the emitted high harmonics from the individual antenna elements forms EUV radiation in the 22-124 nm wavelength range.

A photodetector with smaller active region is faster and has low capacitance. This results in high frequency operation with high output voltage. However, minimizing the photodetector size causes lower responsivity due to the diffraction limit. Miller and colleagues overcome this challenge with the open-sleeve dipole antenna [6]. As seen in figure 2.13, a dipole gold nanoantenna is used to concentrate incident near infrared light into germanium active material. The
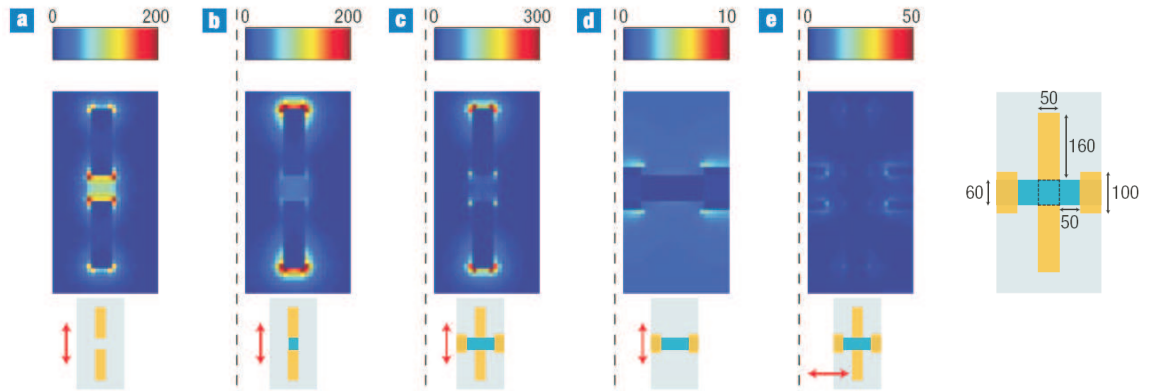
Figure 2.14: Calculated spatial near field on 25 nm above the $SiO_2$ substrate surface, (a) to (d) y polarized illumination. (a) Dipole with an air gap, resonant at $\lambda = 904$ nm. (b) Dipole with the gap filled with germanium, resonant at $\lambda = 1271$ nm. (c) Open sleeve dipole, resonant at $\lambda = 1345$ nm. (d) Open sleeve. (e) Open sleeve dipole, x polarized illumination. [6].

sleeves are used to extract the photocurrent. The measured photocurrent for y polarized incident light is 20 times higher than that for $x$ polarized light at a very low bias voltage at $\lambda = 1310$ nm wavelength. Calculated near field, shown in figure 2.14 predicts this polarization response and proves how the sleeves change antenna characteristics.

Nanoantennas resonating at infrared wavelengths have the potential to collect the infrared energy either coming from the sun or reradiated from the earth. However, this is impossible for the time being due to the lack of terahertz rectification of the induced current on nanoantennas. Nevertheless, Kotter *et al* fabricate inexpensive, flexible and large area periodic array of square loop gold nanoantennas resonating at infrared wavelengths [7]. Figure 2.15 shows the nanoantenna collector sheet. Thus, with the improvement of proper terahertz rectification techniques nanoantennas can be used to extend the limits of conventional photovoltaic technology.
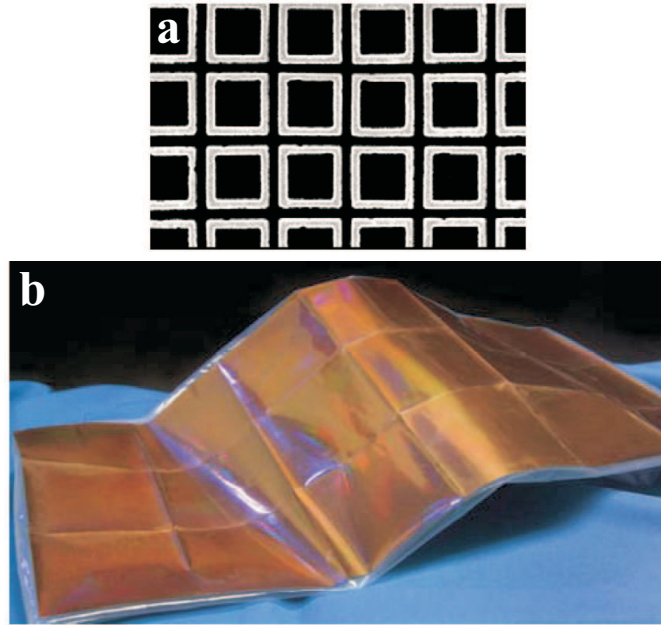
Figure 2.15: (a) SEM image of the square loop antenna array. (b) Nanoantenna collector sheet. [7].

Nanoantennas are also used in biological sciences for example by utilizing them in photothermal tumor therapy [8]. Polyethylene glycol (PEG) coated gold nanorods (NR) resonating at $\lambda = 810$ nm are synthesized, shown in figure 2.16(A). PEG-NRs are stable in biological media and are passively accumulated in tumors through permeability. 72 hours after injection to mice, PEG-NRs disappear from blood circulation. After vascular disappearance of PEG-NRs, tumors of mice are irradiated with a laser of intensity 2 $W/cm^{-2}$ at $\lambda = 810$ nm for 5 minutes. The calculated temperature for three different tumor depths of PEG-NR injected mice and the measured thermographic trace is shown in figure 2.16(B) and (C). Thus laser illumination causes PEG-NRs to heat up by means of the electric field enhancement discussed priorly and ablate the tumor tissue. Figure 2.17 presents the experiment results including the response of control groups. This promising work demonstrates tumor ablation by using nanoantennas as tumor specific catheters.
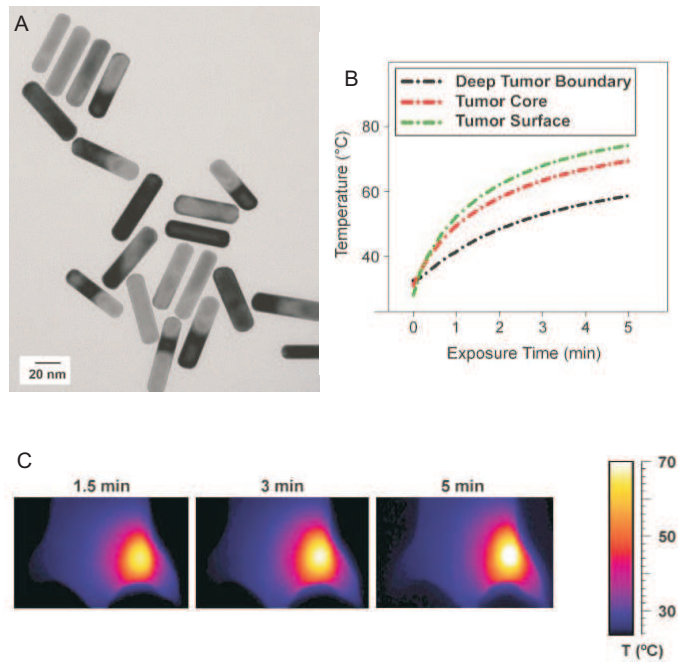
Figure 2.16: (A) TEM image of $13nm \times 47nm$ synthesized gold nanorods. (B) Calculated temperature for three different tumor depths of PEG-NR injected mice. (C) Thermographic imaging of laser irradiated PEG-NR injected mice. [8].
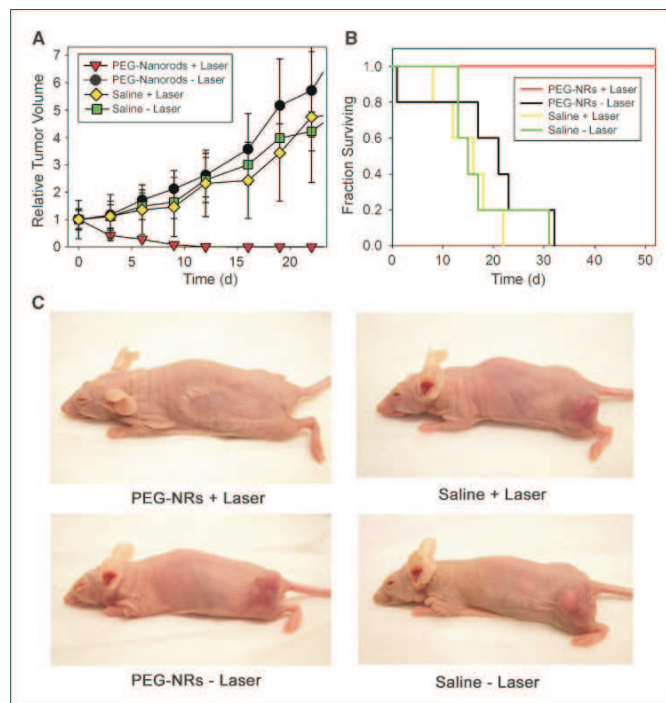


Figure 2.17: Response of different treatment groups (A) Volumetric changes in tumor sizes after laser irradiation at $\lambda = 810$ nm, $2$ $W/cm^{-2}$ intensity, for 5 minutes. (B) Survival of treatment groups after laser irradiation (C) At 20 d after laser irradiation, PEG-NR injected mice is tumor free. [8].

| A. Type | Substrate | A. Length | Mode | Wavelength | Ref. |
|---|---|---|---|---|---|
| Dipole | Glass | 255 nm (20 nm gap) | $\lambda_e ff/2$ | 830 nm | [1] |
| Stripe | Glass | 500 nm | $3\lambda_e ff/2$ | 710 nm | [2] |
| Dipole | Glass | 1040 nm (40 nm gap) | $3\lambda_e ff/2$ | 730 nm | [2] |
| Stripe | Glass | 1000 nm | $5\lambda_e ff/2$ | 760 nm | [2] |
| Dipole | Glass | 380 nm (60 nm gap) | $\lambda_e ff/2$ | 904 nm | [6] |

Table 2.1: Antenna type, substrate, antenna length, resonant mode and wavelength of the incident light in references tabulated.

Table 2.1 lists antenna type, substrate, antenna length, resonant mode and incident wavelength within the aforementioned references for comparison. Here we first infer the directly proportional relation between the incident wavelength and the required antenna length for $\lambda_e ff/2$ resonant mode (first resonance). This characteristics proves that freely accelerating electrons of the nanoantenna are driven by the incident harmonic electromagnetic field and resonate for a specific antenna length. In accordance with the macro antenna theory, the relation between incident wavelength and resonant antenna length is explained with the dynamic current distribution on the antenna, and longer incident wavelengths require longer antennas. Secondly, we deduce that the resonance characteristics of a dipole nanoantenna is governed by individual nano stripes forming the dipole. Neglecting the small coupling effect between individual nano stripes, the dipole behavior is attributed to the stripe nanoantennas due to their individual current distributions in response to the driving field. The coupling due to the small gap increases the resonating wavelength of the individual stripe or in effect increases the effective wavelength ($\lambda_e ff$). Finally, we realize that $\lambda_e ff$ of higher order resonant modes (i.e. $3\lambda_e ff/2$ and $5\lambda_e ff/2$ modes) are longer. We can imagine higher order modes as series combinations of nanoantennas resonating at $\lambda_e ff/2$ mode. However, that series combination has the maximum coupling between those serial elements and thereby lengthens $\lambda_e ff$ of higher order modes.

# Chapter 3

# NUMERICAL CALCULATIONS

In this chapter, nanoantenna and optical field interaction is investigated using industry standard commercial simulation software (Lumerical FDTD). Here we demonstrate the capability of nanoantennas in localized enhancement of light depending on their size, shape and surface properties. We first provide the near field response of various nanoantennas for $\lambda = 1.5~\mu m$ linearly polarized incident optical radiation. Then, we describe the interaction of the optical field ($\lambda = 1.5~\mu m$ incident radiation), resonant stripe nanoantenna and $As_2Se_3$ (arsenic selenide) substrate. Finally, we investigate the electromagnetic field interactions with a resonant stripe nanoantenna placed on a nonlinear (optical) $As_2Se_3$ substrate, concentrating on the nonlinear optical interaction of the antenna near field with the substrate. Lumerical FDTD software allows implementation of the third order susceptibility term $\chi^{(3)}$ and solves nonlinear FDTD. Since $As_2Se_3$ is a highly nonlinear material ($\chi^{(3)} = 6.84 \times 10^{-19}$ at $\lambda = 1.5~\mu m$), higher order effects such as the generation of new frequencies and harmonics, which require very large electric fields to become observable, can be induced with the electromagnetic enhancement achieved via resonant nanoantennas.
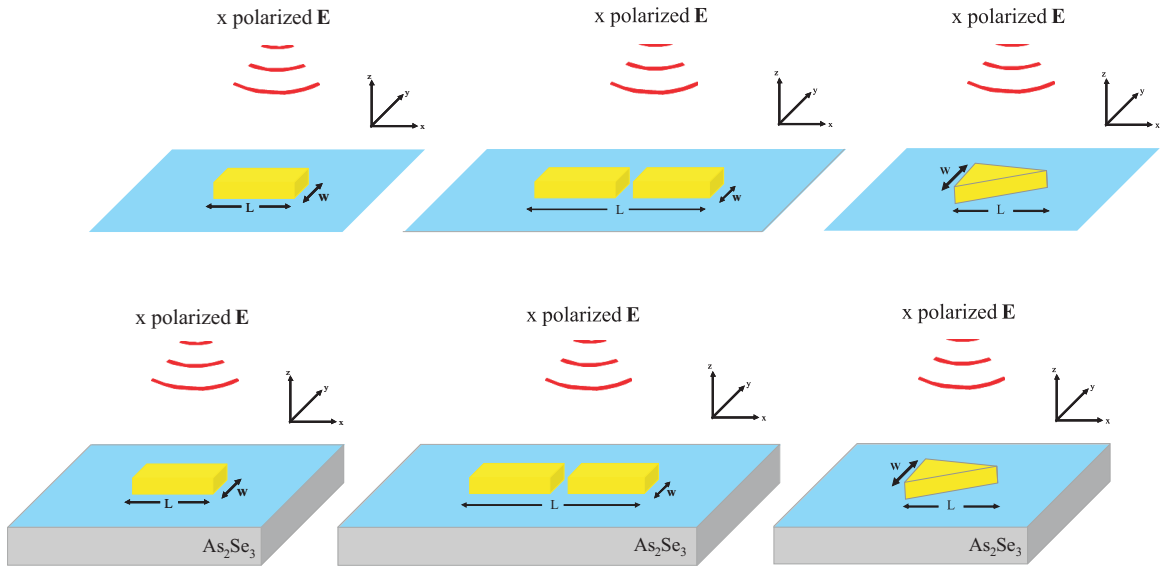
Figure 3.1: Setups and reference frame used in numerical calculations, $L$ is the antenna length, $w$ is the antenna width.

## 3.1 Optical Nanoantennas at $\lambda = 1.5\ \mu m$

In this section, we investigate stripe, dipole and single bow-tie gold nanoantennas for various antenna lengths. Steady state time averaged near field response of these three antenna types is calculated at the bottom face of the antennas for two different cases: when the antenna is in vacuum and when the antenna is on $As_2Se_3$ (arsenic selenide, $n = 2.78$ at $\lambda = 1.5\ \mu m$). Calculated spatial near field intensity is normalized with respect to the incident optical field. The incident light is a transverse electric field linearly polarized in the $x$ direction at a wavelength of $\lambda = 1.5\ \mu m$ with 100 nm bandwidth. Figure 3.1 demonstrates setups and reference frame used in simulations. The blue surface represents the near field monitor at $\lambda = 1.5\ \mu m$. $L$ refers to antenna length and $w$ refers to antenna width. All the calculations are made for fixed antenna width of $w = 50$ nm, except for the bow-tie nanoantenna where $w = 100$ nm is employed. Antenna thickness is always taken as 50 nm. Furthermore, 2 nm mesh size is used in all directions. In order to prevent reflections from the simulation boundaries,
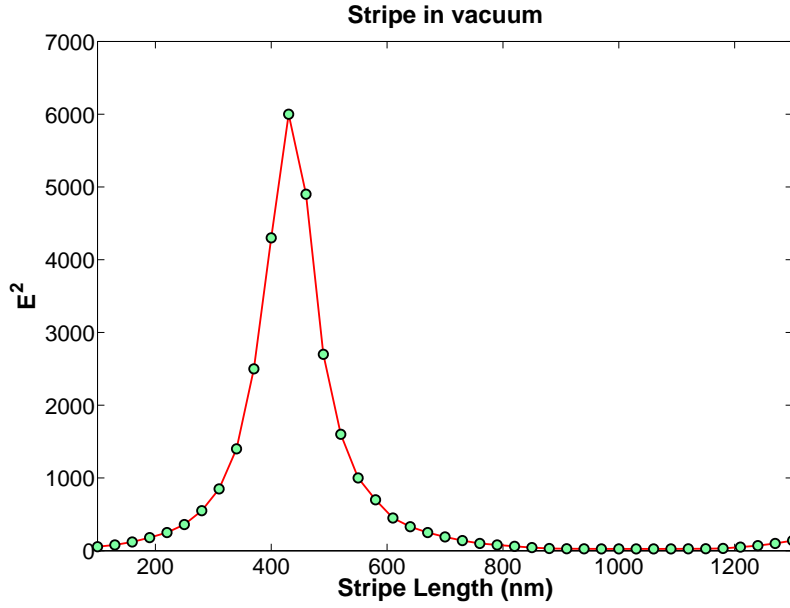
Figure 3.2: Electric field peak intensity calculated for various lengths of the stripe nanoantenna in vacuum.

perfectly matched layers are utilized. Proper convergence is assured for each of the calculations.

The length of the stripe nanoantenna is scanned from 100 nm to 1300 nm with steps of 30 nm. Simulated dipole nanoantenna is comprised of two identical stripes with a constant 40 nm gap; therefore the dipole length is scanned from 240 nm to 2640 nm with 60 nm steps for comparison with the stripe antenna characteristics. Finally, the bow-tie response is calculated for the antenna lengths beginning from 100 nm up to 700 nm again with 30 nm steps.

Here we first provide the calculation results of the nanoantennas in vacuum. Figure 3.2 shows that the stripe nanoantenna in vacuum provides near field enhancement for a band of antenna lengths ceiling at about $L = 430$ nm which is shorter than $\lambda/2$. Therefore, an effective wavelength where $L = \lambda_{eff}/2 = 430$ nm can be defined. Another near field intensity enhancement peak for $L = \lambda_{eff}$ is not observed as predicted by Ghenuche *et al* [2]. Spatial near field distribution for $L = 430nm$ shown in figure 3.3 suggests that the field enhancement is a resonant

Figure 3.3: Electric field intensity distribution of the stripe nanoantenna in vacuum for antenna length of $L = 430$ nm. First resonant mode is presented for two different intensity scales.

Figure 3.4: Electric field peak intensity calculated for various lengths of the dipole nanoantenna in vacuum.

one. At resonance, up to three orders of magnitude intensity enhancement and strong field confinement is observed.

Calculated dipole nanoantenna consists of two identical stripes with a 40 nm constant gap. Here $L$ refers to the total length of two identical stripes and gap. Figure 3.4 indicates that the dipole nanoantenna in vacuum holds near field enhancement for a band of antenna lengths ceiling at about $L = 820$ nm. This implies that the dipole response is governed by the characteristics of individual stripes forming the dipole nanoantenna which is a result arrived at table 2.1 as well. However, resonant antenna length of the individual stripes is slightly lowered due to the coupling between them. Furthermore, spatial near field distribution for $L = 820nm$ shown in figure 3.5 suggests that the dipole design contributes to higher near field intensities than of a single stripe inside the gap.

Figure 3.5: Electric field intensity distribution of the dipole nanoantenna in vacuum for antenna length of $L = 820$ nm. First resonant mode is presented for two different intensity scales.

Figure 3.6: Electric field peak intensity calculated for various lengths of the bow-tie nanoantenna in vacuum.

Simulated bow-tie nanoantenna is a single isosceles triangle with height $L$ and base length $w = 100$ nm. Figure 3.6 indicates that the bow-tie nanoantenna in vacuum presents near field enhancement for a band of antenna lengths ceiling at about $L = 430$ nm, which is the same resonant length for nano stripe in vacuum. This implies that the resonance is related to the length of the antenna along the polarization direction of the incident light. As in the case of its radio equivalent, bow-tie nanoantenna is said to be middle bandwidth meaning that the range of frequencies producing resonance like behavior is wider than a lower bandwidth antenna [10]. This can be explained with the following analogy: the bow-tie nanoantenna behaves like a parallel combination of stripe nanoantennas. As a result, figure 3.6 includes more number of antenna lengths producing resonance like behavior and thereby near field intensity enhancement. Furthermore, the near field intensity enhancement of the bow-tie nanoantenna is an order of magnitude higher than the nano stripe. This is attributed to the sharp tip of the bow-tie. Figure 3.7 presents spatial near field distribution for $L = 430$ nm. Hence for an application where a single tiny optical spot of very high intensity is required, a resonant bow-tie design could be employed.
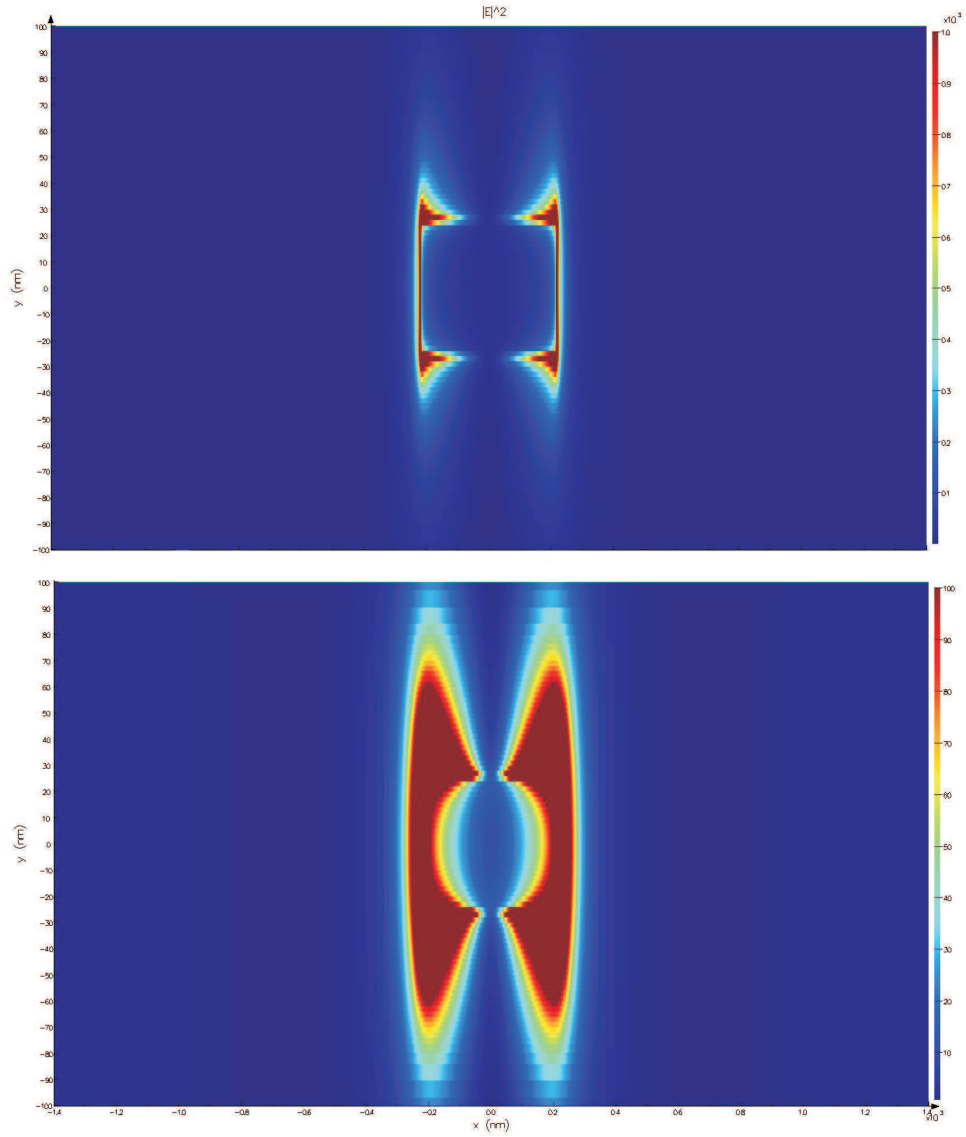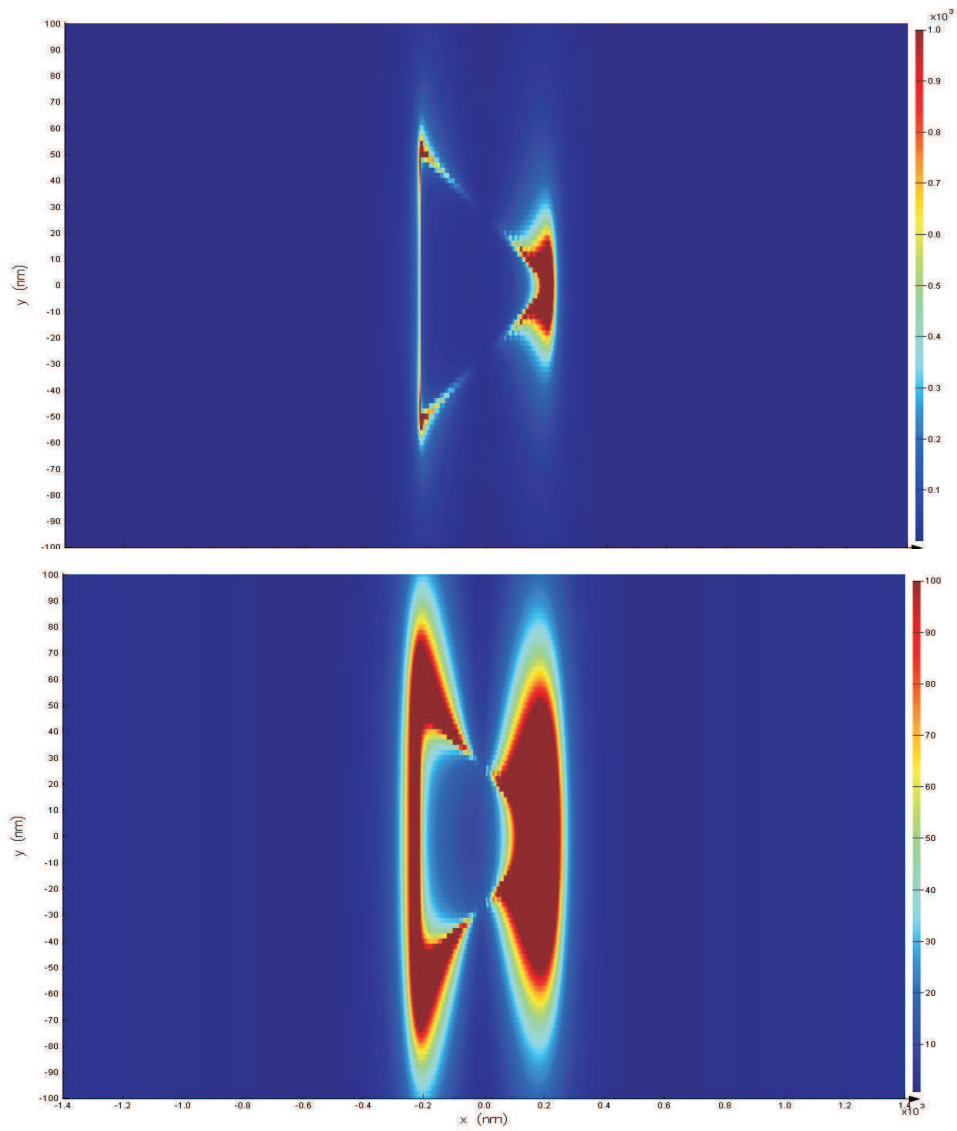
Figure 3.7: Electric field intensity distribution of the bow-tie nanoantenna in vacuum for antenna length of $L = 430$ nm. First resonant mode is presented for two different intensity scales.
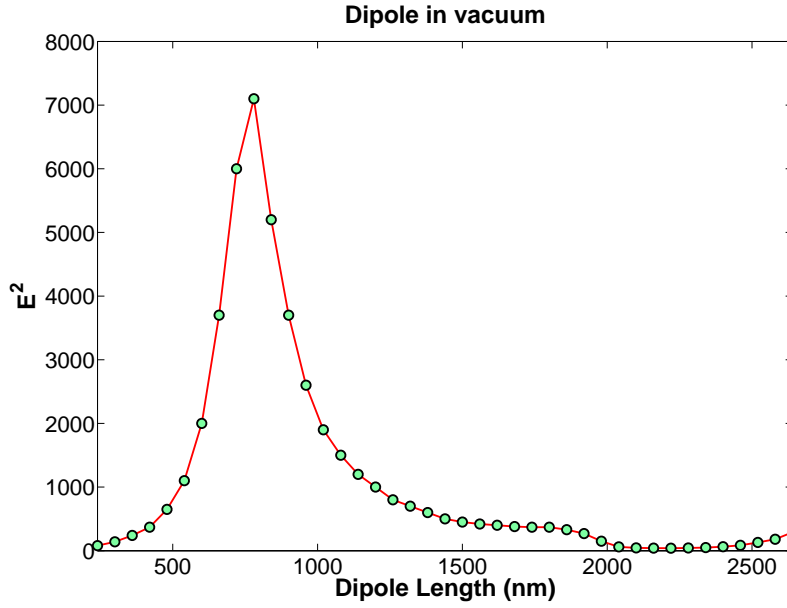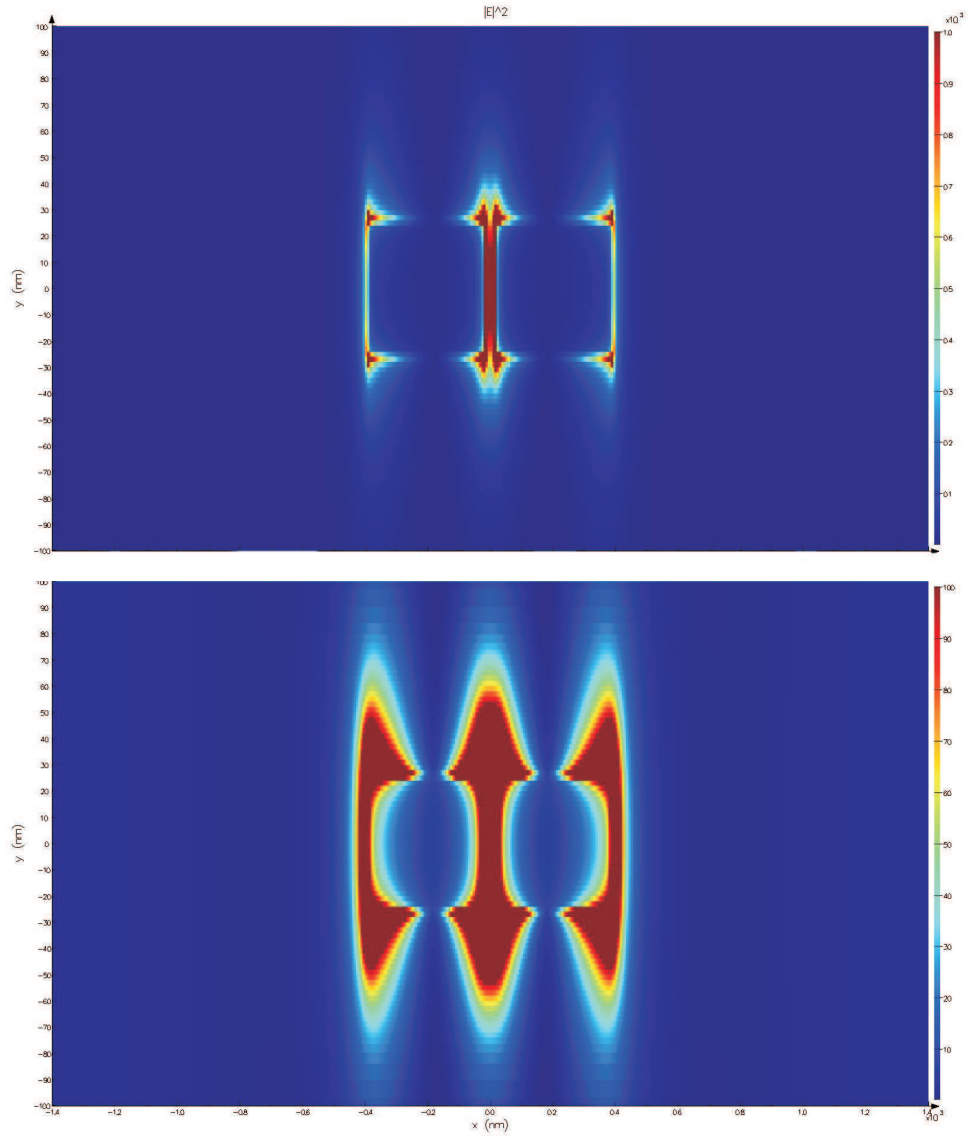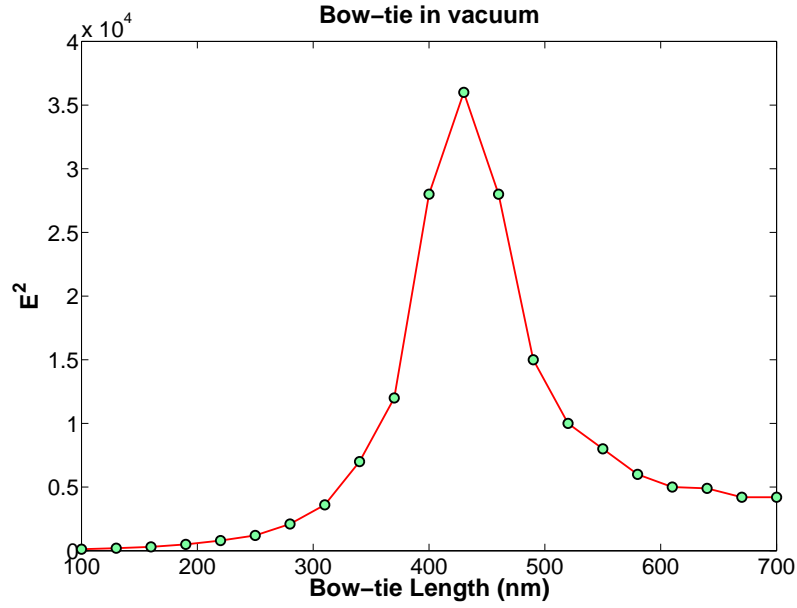
Figure 3.8: Electric field peak intensity calculated for various lengths of the stripe nanoantenna on $As_2Se_3$ substrate.

Regarding the case of nanoantennas on $As_2Se_3$ (arsenic selenide) substrate, figure 3.8 reveals that the stripe nanoantenna on $As_2Se_3$ grasps near field enhancement for several bands of antenna lengths ceiling at about $L = 190$ nm, $L = 670$ nm and $L = 1150$ nm. The dielectricity of the $As_2Se_3$ substrate ($n = 2.78$ at $\lambda = 1.5$ $\mu m$) opposes the dynamic charge distribution on the metal surface and introduces additional capacitance thereby lowering the resonant length of the nanoantenna. Hence we observe higher order resonant modes of the stripe which require longer antennas for the antenna lying in vacuum case. First resonance, so called the fundamental antenna mode, occurs at about $L = 190$ nm, where we can define an effective wavelength, $L = \lambda_{eff}/2 = 190$ nm. Second resonance, $3\lambda_{eff}/2$ mode, occurs at about $L = 670$ nm and third resonance, $5\lambda_{eff}/2$ mode, occurs at about $L = 1150$ nm, all similar to the definition in the work of Ghenuche *et al* [2]. In accordance with table 2.1, $\lambda_{e}ff$ of higher order resonant modes are longer. Furthermore, the dielectricity of the substrate also reduces the strength of resonance and thus decreases the intensity enhancement factor compared to the stripe lying in vacuum. Figures 3.9, 3.10 and 3.11

Figure 3.9: Electric field intensity distribution of the stripe nanoantenna on $As_2Se_3$ substrate for antenna length of $L = 190$ nm. First resonant mode is presented for two different intensity scales.

Figure 3.10: Electric field intensity distribution of the stripe nanoantenna on $As_2Se_3$ substrate for antenna length of $L = 670$ nm. Second resonant mode is presented for two different intensity scales.

Figure 3.11: Electric field intensity distribution of the stripe nanoantenna on $As_2Se_3$ substrate for antenna length of $L = 1150$ nm. Third resonant mode is presented for two different intensity scales.
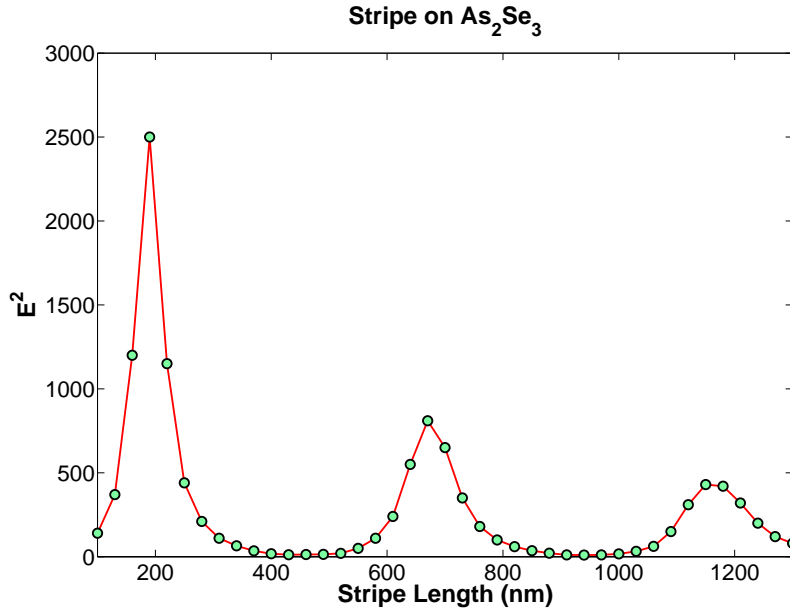
Figure 3.12: Electric field peak intensity calculated for various lengths of the dipole nanoantenna on $As_2Se_3$ substrate.

present spatial near field distributions for three different modes. The fundamental resonant mode is more efficient than higher order modes but its shorter length requires more stringent fabrication methods. Spatial near field distributions suggest that higher order modes can be imagined as series combinations of antennas resonating at the fundamental mode.

Figure 3.12 indicates that the dipole nanoantenna on $As_2Se_3$ provides near field enhancement for several bands of antenna lengths ceiling at about $L = 360$ nm,$L = 1380$ nm and $L = 2340$ nm. As in the case of dipole lying in vacuum, we calculated near field response of two identical stripes with a constant $40nm$ gap. The dipole response is again governed by the characteristics of the individual stripes on $As_2Se_3$. The resonant antenna length of the individual stripes is slightly lowered due to coupling. Furthermore, higher refractive index substrate makes three different resonant modes observable albeit lowering the resonance strength. Dipole nanoantenna on $As_2Se_3$ characteristics is in accordance with the results that we arrive at dipole in vacuum and stripe on $As_2Se_3$ cases. Figures 3.13, 3.14, 3.15 present spatial near field distributions for three different modes.

Figure 3.13: Electric field intensity distribution of the dipole nanoantenna on $As_2Se_3$ substrate for antenna length of $L = 360$ nm. First resonant mode is presented for two different intensity scales.

Figure 3.14: Electric field intensity distribution of the dipole nanoantenna on $As_2Se_3$ substrate for antenna length of $L = 1380$ nm. Second resonant mode is presented for two different intensity scales.
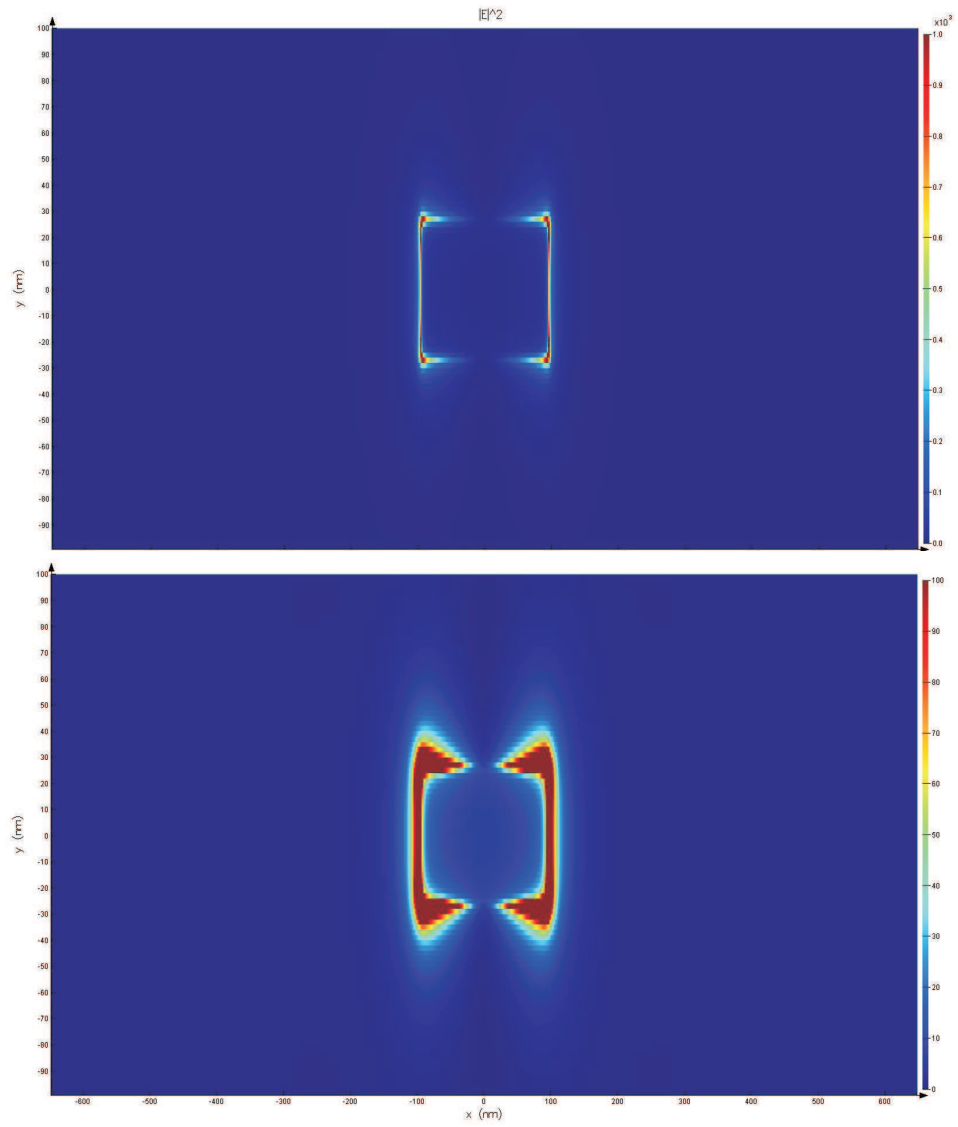
Figure 3.15: Electric field intensity distribution of the dipole nanoantenna on $As_2Se_3$ substrate for antenna length of $L = 2340$ nm. Third resonant mode is presented for two different intensity scales.

Figure 3.16: Electric field peak intensity calculated for various lengths of the bow-tie nanoantenna on $As_2Se_3$ substrate.

Figure 3.15 presenting the third resonant mode should also be noted due to several optical spots of high intensity with nanometer resolution.

Figure 3.16 shows that the single bow-tie nanoantenna on $As_2Se_3$ substrate holds near field enhancement for several bands of antenna lengths ceiling at about $L = 190$ nm and $L = 670$ nm which are expectely the same resonant antenna lengths for the nano stripe on $As_2Se_3$. This demonstrates that the resonance depends on the antenna length along the polarization direction. However, the dielectricity of the substrate reduces the intensity enhancement factor compared to the bow-tie nanoantenna lying in vacuum. Figures 3.17 and 3.18 present spatial near field distributions for two different modes. The optical spots of high intensity in the second order mode are also identical to the second order mode of the nano stripe thereby implying the resonant antenna length as independent from the antenna shape.

Cubukcu *et al* investigates the response of stripe, dipole, single and double bow-tie nanoantennas on glass substrate for $\lambda = 830$ nm incident electric field linearly polarized along the antenna length [9]. The results in figures 3.19 and
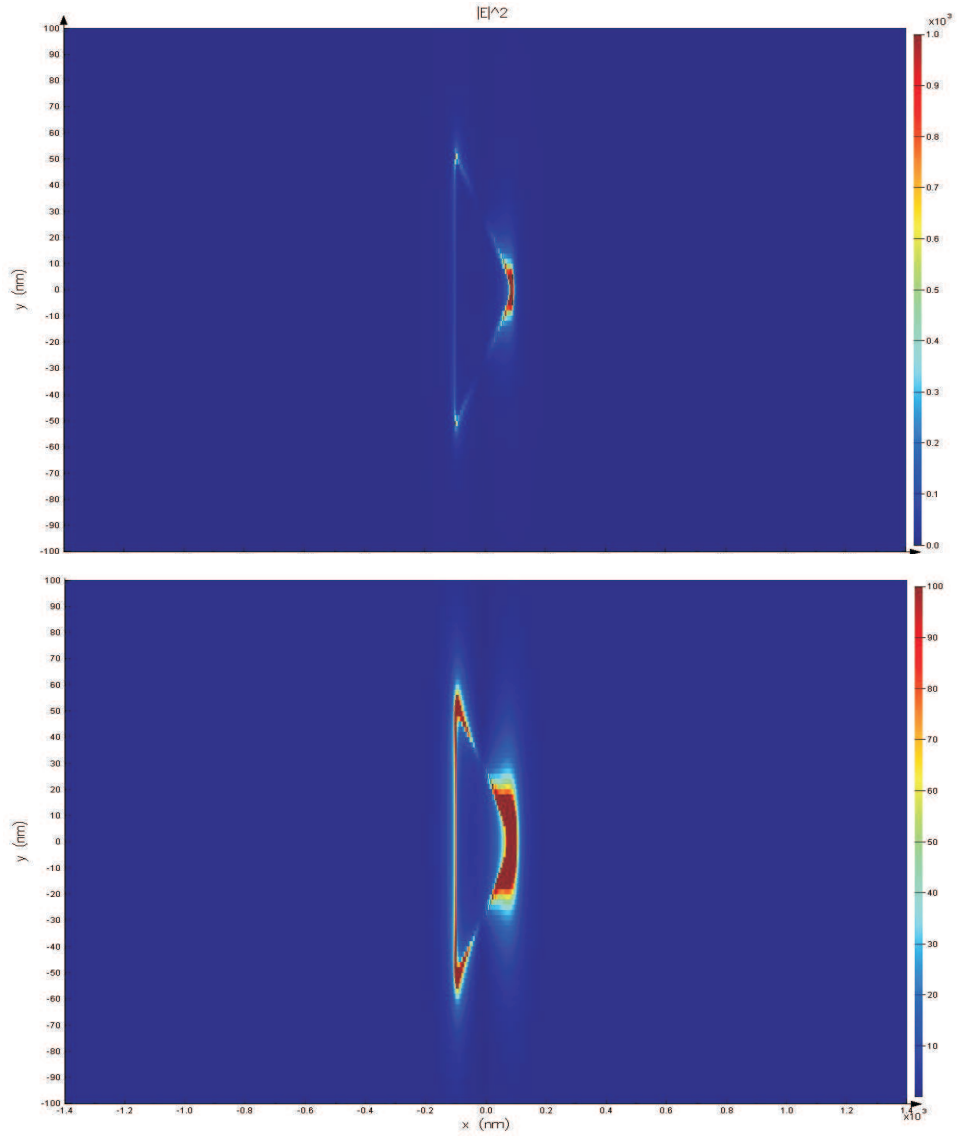
Figure 3.17: Electric field intensity distribution of the bow-tie nanoantenna on $As_2Se_3$ substrate for antenna length of $L = 190$ nm. First resonant mode is presented for two different intensity scales.
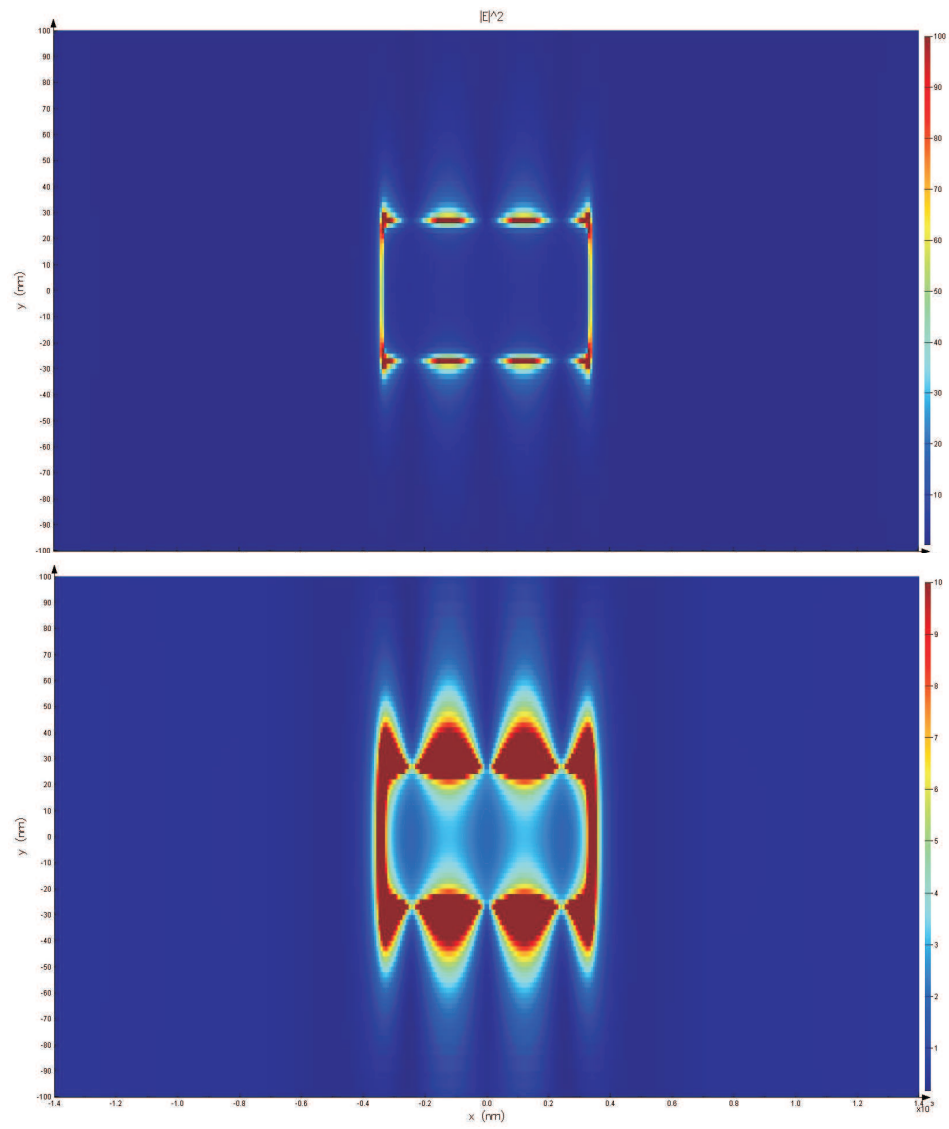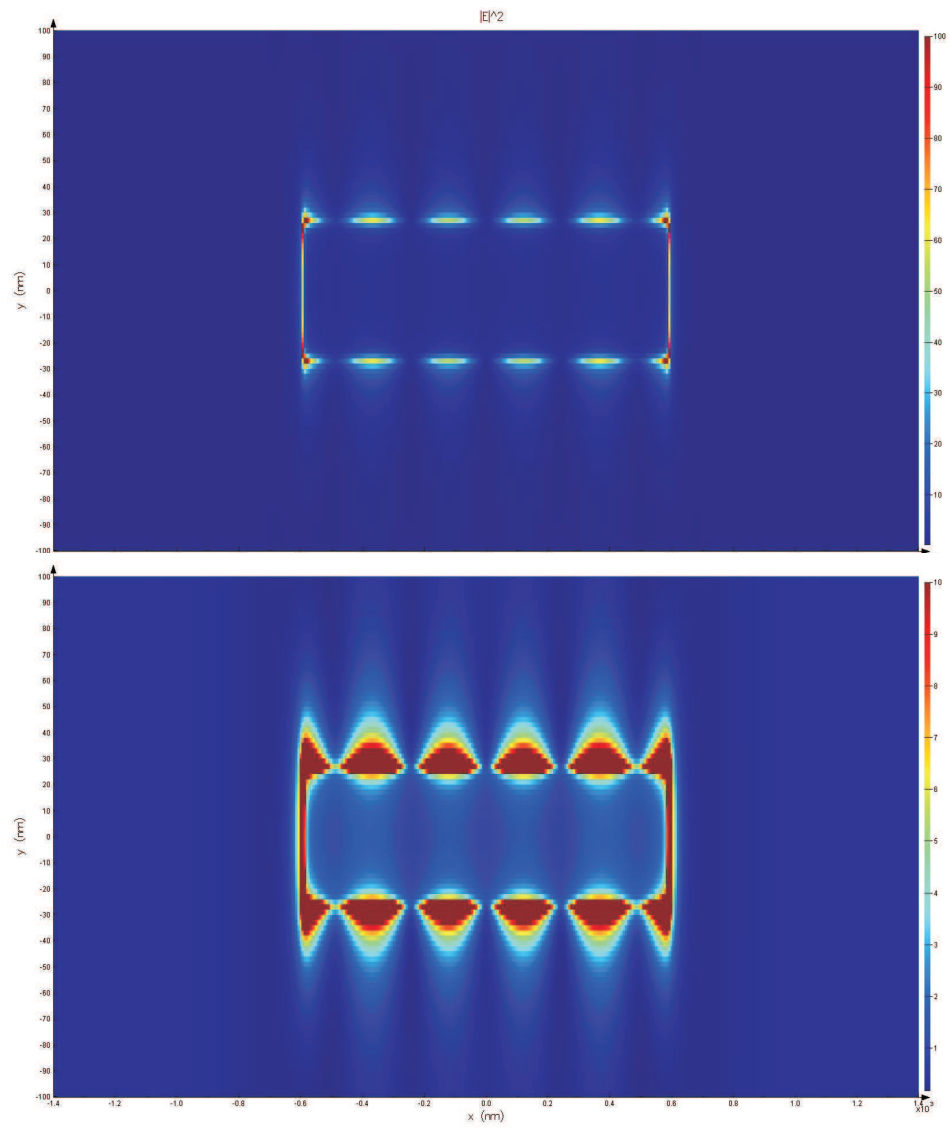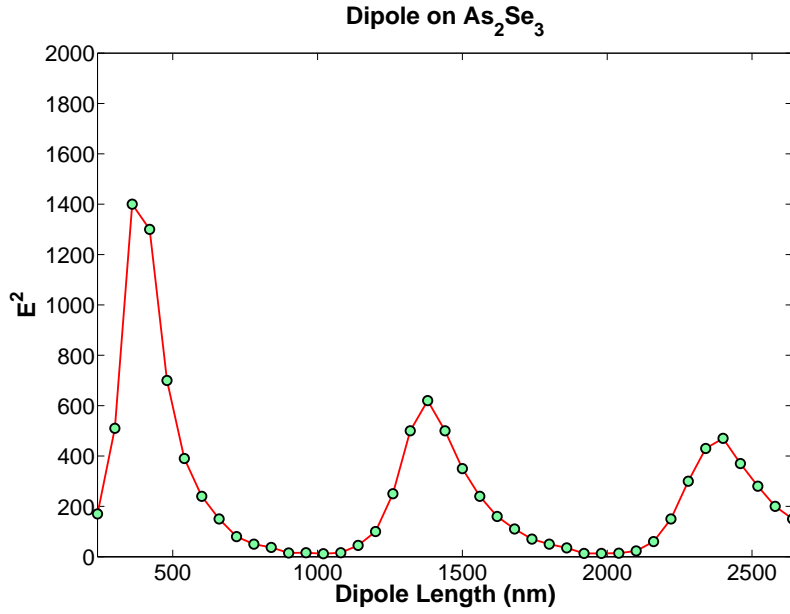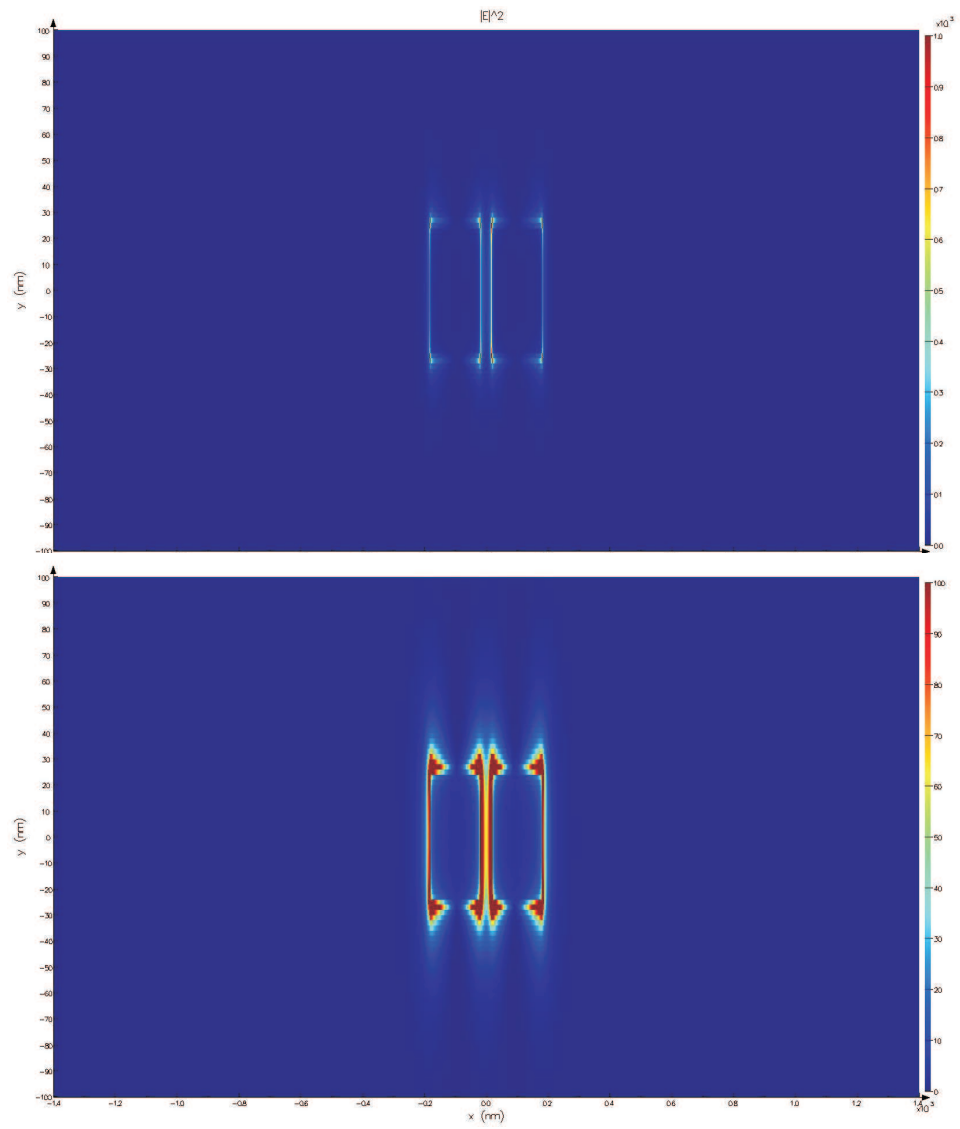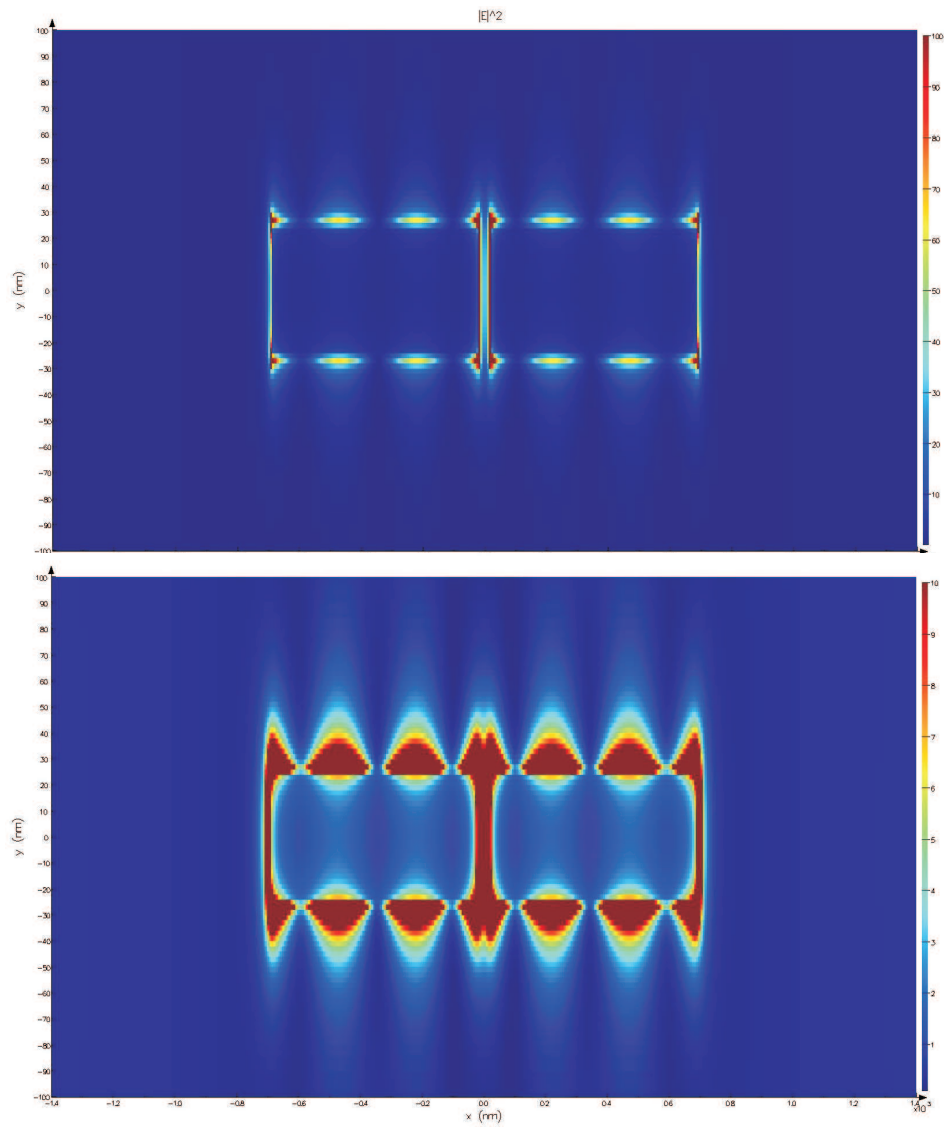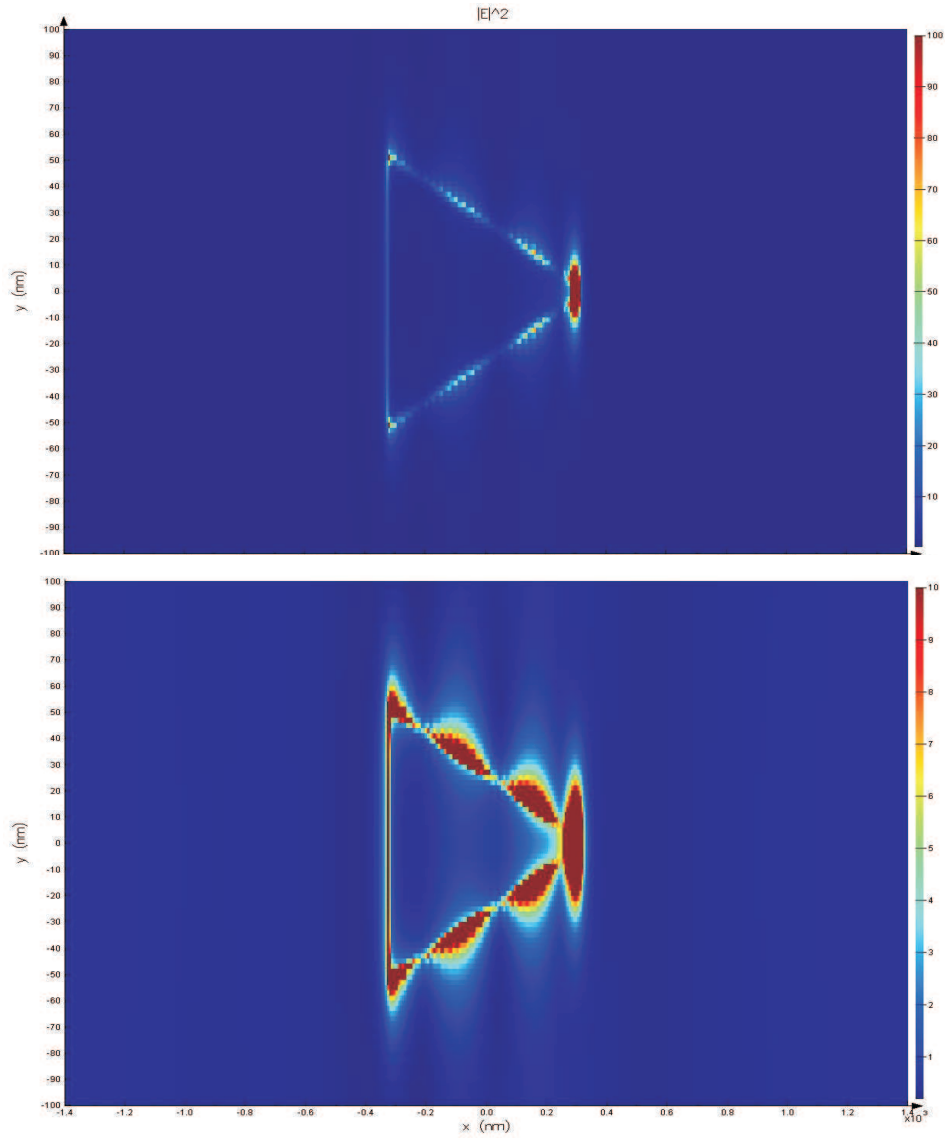
Figure 3.18: Electric field intensity distribution of the bow-tie nanoantenna on $As_2Se_3$ substrate for antenna length of $L = 670$ nm. Second resonant mode is presented for two different intensity scales.
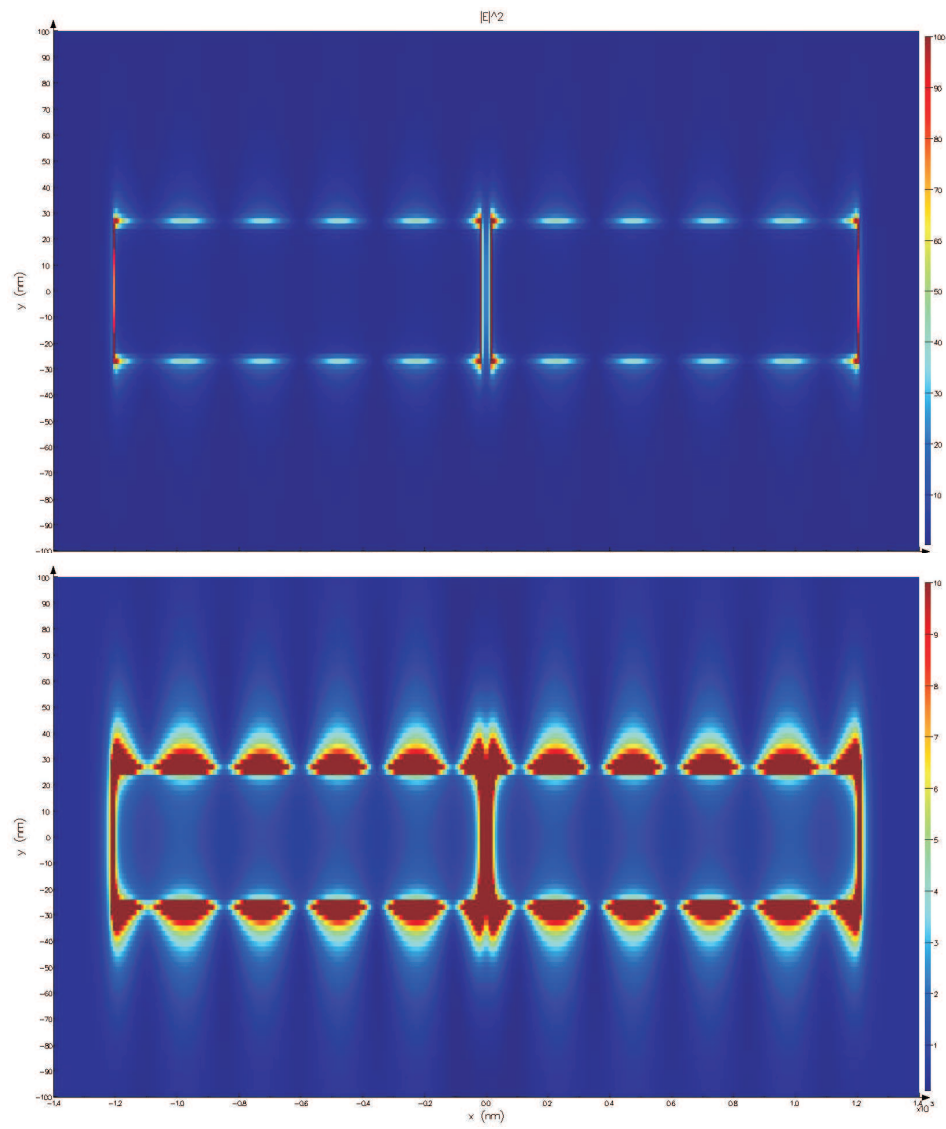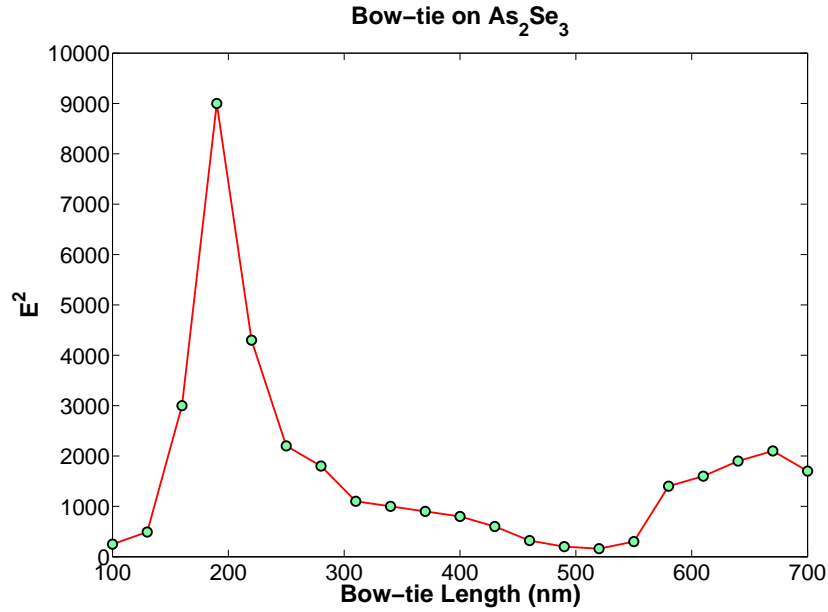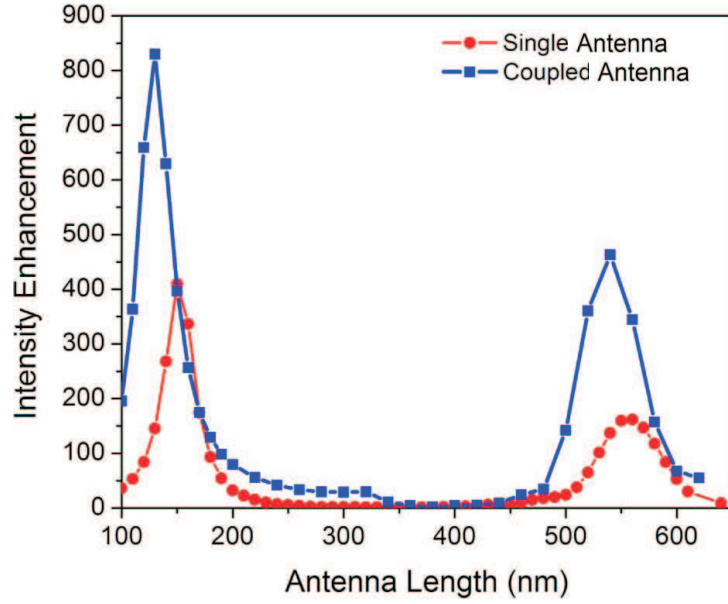
Figure 3.19: Electric field peak intensity calculated for various lengths of stripe and dipole nanoantennas on glass substrate are compared. For the dipole, antenna length is the length of the stripe forming the dipole and the gap is 20 nm [9].

3.20 are in agreement with our numerical calculations. However, the resonant lengths of the stripe (dipole) and single bow-tie (double bow-tie) nanoantennas do not coincide due to the curvature of the simulated structures. The ends of stripe along its length are rounded with a 20 nm radius of curvature, and the tip radius of curvature for bow-tie is taken to be 10 nm with an apex angle of 60°.

As a result of the above numerical calculations we show that resonance characteristics of nanoantennas for a specific incident wavelength is governed by substrate, antenna length along the polarization direction of the incident electric field and the antenna shape. The refractive index of the substrate is inversely proportional with the resonant nanoantenna length and the near field intensity enhancement factor at resonance. This result is compatible with table 2.1, which tabulates simulation results for resonant nanoantennas on glass substrate. Furthermore, a specific incident wavelength causes resonant modes only for specific nanoantenna lengths. This result is also compatible with table 2.1 which manifests a directly proportional relation between the incident wavelength and the
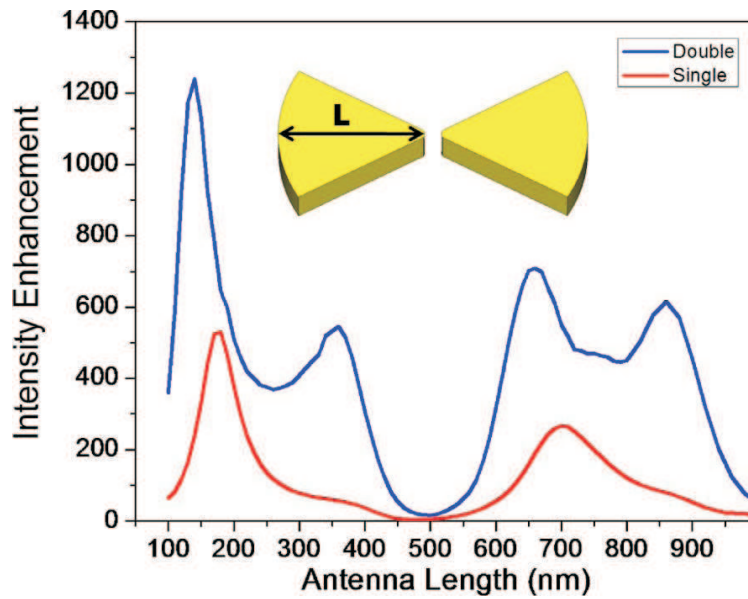
Figure 3.20: Electric field peak intensity calculated for various lengths of single and double bow-tie nanoantennas on glass are compared. For the double bow-tie, antenna length is the length of the single bow-tie forming the double bow-tie and the gap is 20 nm [9].

resonant antenna length. Finally, the nanoantenna shape does not alter the resonant antenna length fundamentally as long as the antenna length along the polarization of the incident field is preserved. However, the shape prominently affects near field intensity enhancement and antenna bandwidth.
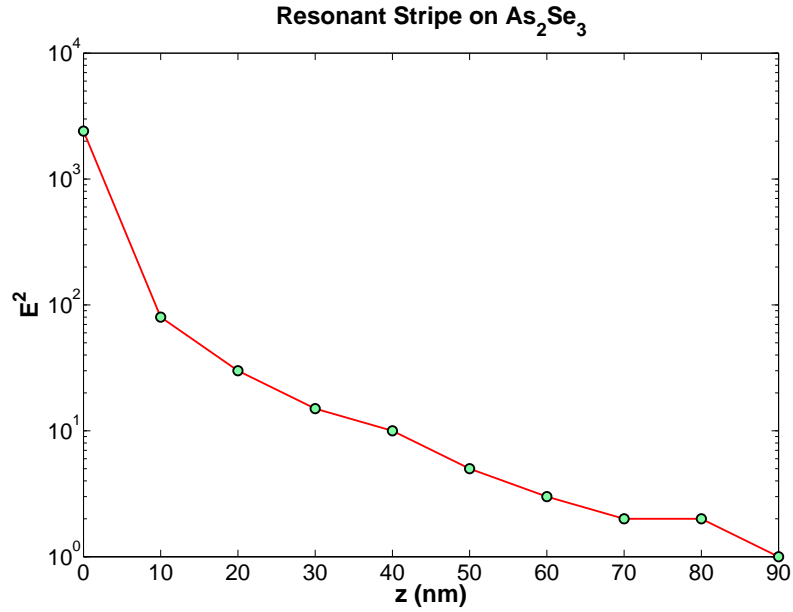
Figure 3.21: Electric field peak intensity calculated for several distances from the antenna dielectric interface for the fundamental resonance mode of the stripe nanoantenna on $As_2Se_3$ (arsenic selenide) substrate.

## 3.2    Resonant Stripe Nanoantenna on $As_2Se_3$

This section describes the interaction of the optical field, stripe nanoantenna at the fundamental resonance mode ($\lambda = 1.5\ \mu m$, $x$ polarized incident radiation) and $As_2Se_3$ substrate.

The interface between the resonating antenna and dielectric substrate is exposed to high electric field intensities albeit the penetration of that field into the dielectric is limited. As seen in figure 3.21, the near field enhancement of the resonating antenna vanishes about 90 nm away from the interface. This result is consistent with the rapid energy decay rate of the reactive near field region and demonstrates strong field confinement inside several cubic micrometers instead of propagation. Therefore, the resonating nanoantenna is a means for optimum conversion of propagating light into subwavelength localized optical field.

We also investigate components of the electric field intensity calculated at the antenna dielectric interface in order to understand nanoantenna radiation in general. Figure 3.22 shows field components of the resonating stripe nanoantenna. Interestingly, all three of $E_x{}^2$, $E_y{}^2$ and $E_z{}^2$ have similar peak intensities albeit their distributions are different. This phenomenon can be described by a simple model assuming electrons of the antenna as freely accelerating and driven by the incident harmonic electromagnetic field. This assumption vanishes the friction term $\gamma$ in equation 2.3 (that is proportional to velocity) without fundamentally changing the resonance phenomena. Furthermore, in order to qualitatively discuss the phenomena we should only consider first order effects due to the electric and magnetic field components of the incident field on the acceleration of the free charges. Here we ignore secondary interactions due to the charge radiation field and charges themselves. FDTD solutions take into account this secondary and higher order interactions due to the induced fields to obtain a converging solution.

As indicated in chapter 2, the electromagnetic radiation from a freely accelerating charge, for example in a plasma, known as the Larmor radiation, is directed perpendicular to the acceleration direction and shaped like a toroid centered around the symmetry axis of the particle's acceleration direction. Therefore, for $x$ polarized incident electric field, the direction of resonant nanoantenna radiation should be around a toroid centered along the antenna axis. This leads to very large $E_y$ and $E_z$ components, and a small but finite contribution from $E_x$. In figure 3.22 we already see prominent $E_y{}^2$ and $E_z{}^2$ components. However we should also be able to account for reasonably large $E_x$ component. This can be attributed to the $y$ polarized magnetic field component of the incoming field. The magnetic force on the charges moving along the $x$ axis is along the $z$ direction because of the Lorentz force relation

$$F = -q\dot{x} \times B(t). \tag{3.1}$$

Therefore, as $x$ polarized incident electric field accelerates the charges along the $x$ axis, $y$ polarized magnetic field bents the charge motion towards the surface and bottom of the antenna harmonically, resulting acceleration along the $z$ axis as well. An acceleration in the $z$ direction is also accompanied with radiation field components $E_x$ and $E_y$. However, magnetic forces are several orders of magnitude smaller than electric forces. Therefore, exact computation of field components requires detailed numerical calculations.

It is interesting to note that the $E_x{}^2$ and to an extent $E_y{}^2$ components in figure 3.22 have another very weak pairs of hot spots at the center of the nanoantenna in distinction to the $E_z$ component suggesting that the source of this hot spots are different. Furthermore, the higher order resonant modes mentioned in the previous section mainly have enhanced $E_y$ and $E_z$ type hot spots which is suggesting that the resonance behavior of the nanoantenna is due to the main resonance along the antenna length.

The relative strengths of the field components depend on many factors affecting the resonance condition, i.e. antenna length and also width. Field strengths and computation eventually require simulation software. However, via our toy model, we show that we can account for the $E_x{}^2$, $E_y{}^2$ and $E_z{}^2$ components by taking into account the electron acceleration due to $E_x$ and $B_y$ components of the incident optical field.
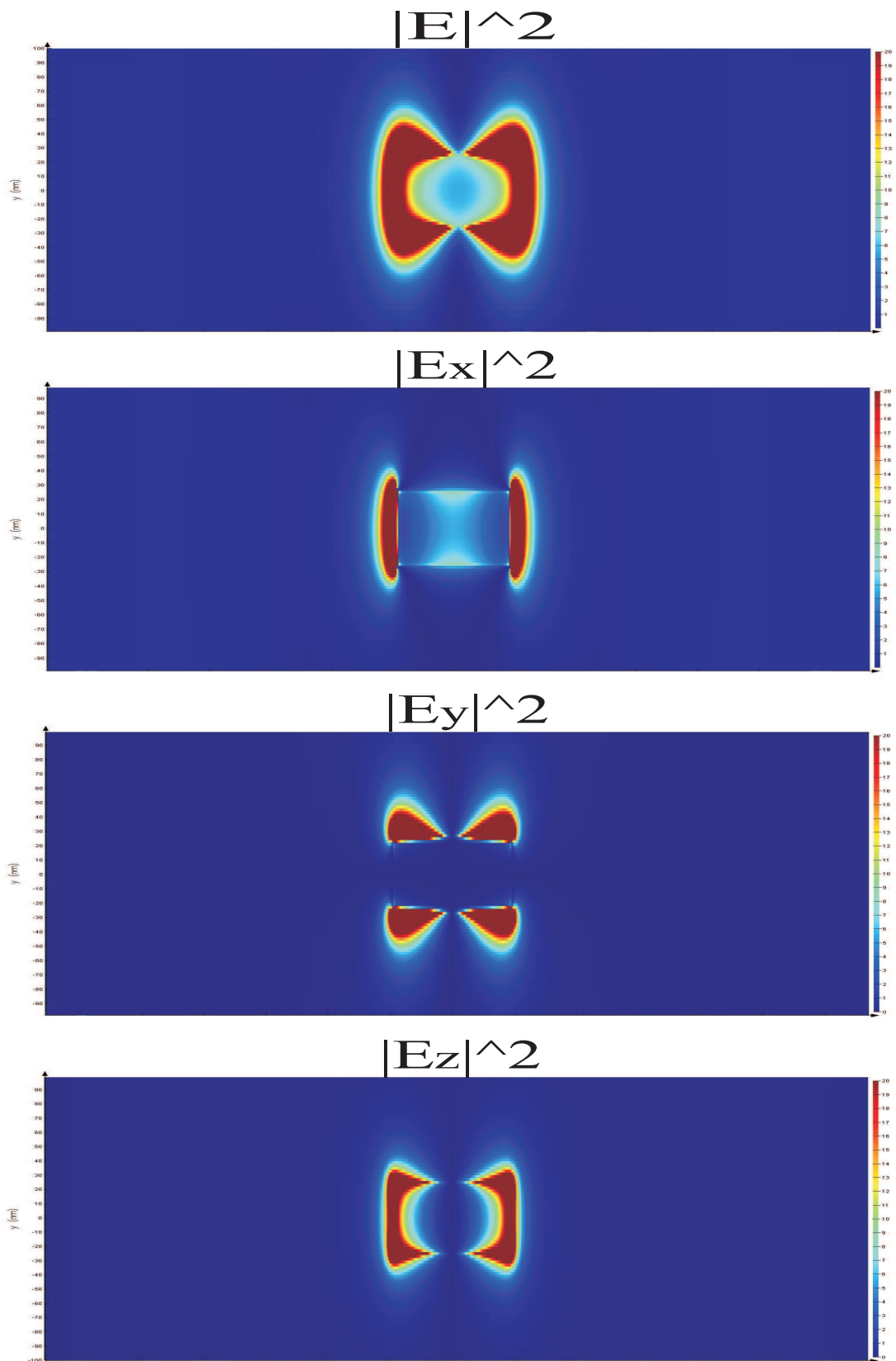
Figure 3.22: Electric field intensity distribution in terms of field components for the fundamental resonance mode of the stripe nanoantenna on $As_2Se_3$.

## 3.3 Resonant Stripe Nanoantenna on $As_2Se_3$ and Nonlinear Effects

This section describes the interaction of high intensity optical field, stripe nanoantenna at the fundamental resonance mode ($\lambda = 1.5$ $\mu m$, $x$ polarized incident radiation) and nonlinear (optical) $As_2Se_3$ (arsenic selenide) substrate.

Local optical field enhancement of resonant nanoantennas can be used for boosting nonlinear phenomena in the nano scale [1, 2, 5]. Since nonlinear effects require very large electric fields to become observable, the near field enhancement achieved around several cubic micrometers of resonant nanoantennas can be exploited for the generation of new frequencies and harmonics. $As_2Se_3$ is a highly nonlinear (optical) material ($\chi^{(3)} = 6.84 \times 10^{-19}$ at $\lambda = 1.5$ $\mu m$) especially used in nonlinear fiber devices [29]. Here we investigate nonlinear optical interactions within the near field of a resonant stripe nanoantenna placed on $As_2Se_3$ substrate.

Lumerical FDTD allows implementation of the third order susceptibility term $\chi^{(3)}$ and solves nonlinear FDTD. Here, the calculation is performed with incident transverse electric field (at $\lambda = 1.5$ $\mu m$) polarized along the antenna length. The incident field is a single pulse of peak amplitude $1e8$ V/m with duration in the order of femtoseconds. The electric field intensity at the antenna dielectric interface is monitored during the pulse transition, and then transformed into the frequency domain by fast fourier transformation. As a result, position and wavelength dependent electric field intensity plots of the antenna dielectric interface are obtained.

Figures 3.23, 3.24, 3.25 and 3.26 present electric field intensity spectrum along a line, in the $x$ direction, grazing the top left corner of the antenna. Therefore, all of the plots are given for the same $y = 25$ nm position. The 190 nm long and

Figure 3.23: $E_x{}^2$ spectrum calculated at different $x$ positions. The source has 150 fs pulse length at 1.5 $\mu m$. $E_x{}^2$ is normalized with respect to the source peak intensity.

50 nm wide resonant nanoantenna lies between $x = -95$ nm and $x = 95$ nm $x$ and $y = -25$ nm and $y = 25$ nm $y$ positions of the simulation area. Since near field response of the nanoantenna is symmetrical in the $xy$ plane with respect to the antenna center, electric field intensity spectrum at different $x$ points along the top edge of the antenna up to $x = 0$ is sufficient to analyze the phenomenon.

The wavelength spectrum is restricted in the 400 nm to 2000 nm range, and normalized with respect to the peak intensity of the incident field. The calculations are made for two different pulse lengths of 150 fs and 300 fs. Furthermore, $E_x{}^2$ and $E_y{}^2$ spectrum are given separately for each of the different incident pulse lengths. Since the third order optical nonlinearity of $As_2Se_3$ is isotropic, sufficient field intensity provided by the source and enhanced by the resonant nanoantenna produces nonlinear effects in terms of both $E_x$ and $E_y$ field components.
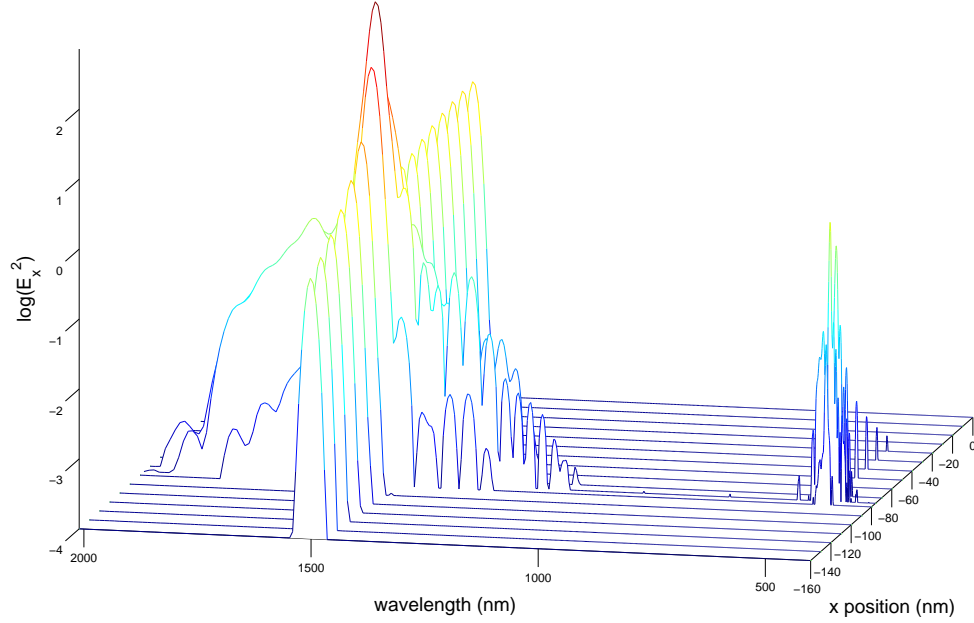
51

Figure 3.24: $E_y{}^2$ spectrum calculated at different $x$ positions. The source has 150 fs pulse length at 1.5 $\mu m$. $E_y{}^2$ is normalized with respect to the source peak intensity.

Figure 3.23 shows $E_x{}^2$ spectrum in the logarithmic scale for 150 fs incident pulse length. At points far from the antenna edge ($x < -95$) electric field enhancement is not sufficient for nonlinear generations. At points closer to the antenna edge, more than two orders of magnitude intensity enhancement is naturally observable at 1500 nm, which is the resonating wavelength of the nanoantenna. Due to sufficient resonant field enhancement, nonlinear interactions give rise to new frequency components in the neighborhood of the antenna edge where near field intensity enhancement is maximum. Third harmonic of the resonating wavelength, 500 nm, also clearly appears at $x = -95$ nm and decays away from the antenna edge. Hence the appearance of new frequencies around 1500 nm and the third harmonic generation at 500 nm shown in the spectral plot are in accordance with the $x$ polarized resonant near field enhancement. Since the antenna
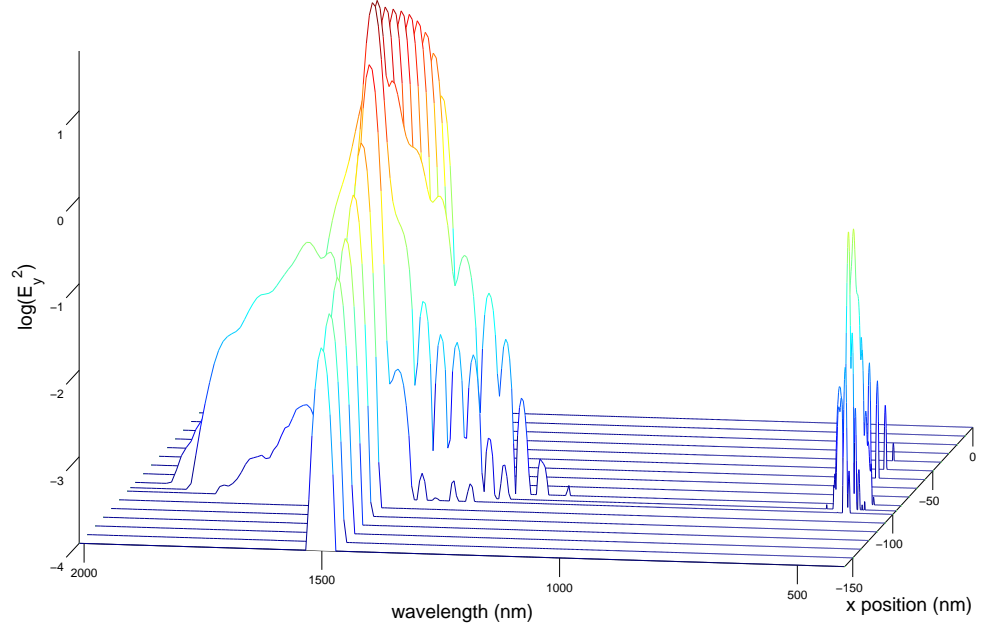
Figure 3.25: $E_x{}^2$ spectrum calculated at different $x$ positions. The source has 300 fs pulse length at 1.5 $\mu m$. $E_x{}^2$ is normalized with respect to the source peak intensity.

does not have a resonating mode other than $\lambda = 1500$ nm, nonlinear generations are not amplified.

Figure 3.24 shows $E_y{}^2$ spectrum in the logarithmic scale for 150 fs incident pulse length. Since $E_x{}^2$ and $E_y{}^2$ intensity enhancement distributions of the resonant nanoantenna are different as described in the previous section, $E_y{}^2$ spectrum representing the $y$ polarized nonlinear generations differs from the $E_x{}^2$ spectrum in this respect. For instance, the generated third harmonic at 500 nm does not decay with distance from the corner of the antenna as fast as in figure 3.23. Therefore, near field of the resonant nanoantenna can be used as position dependent and polarized source for nonlinear interactions.
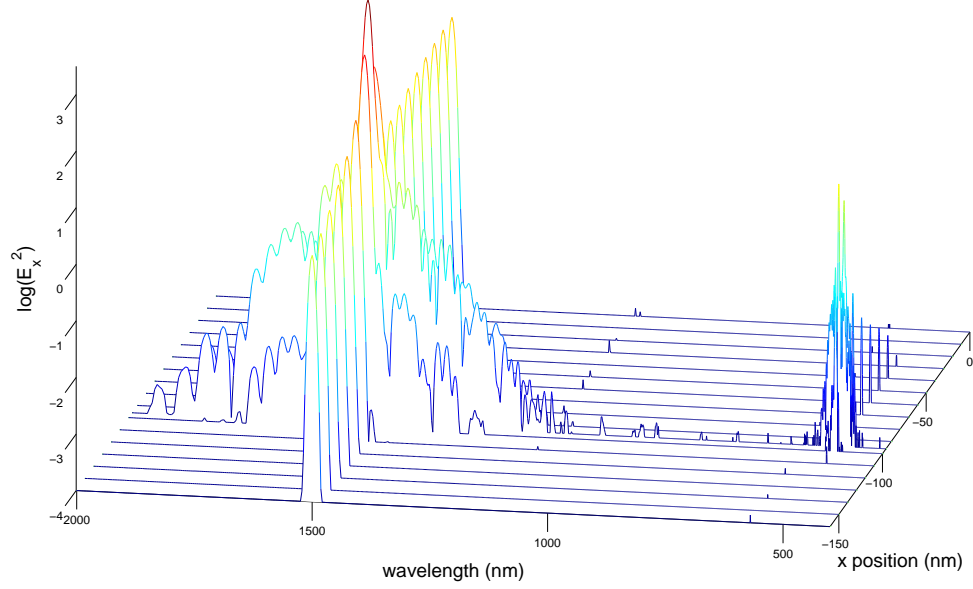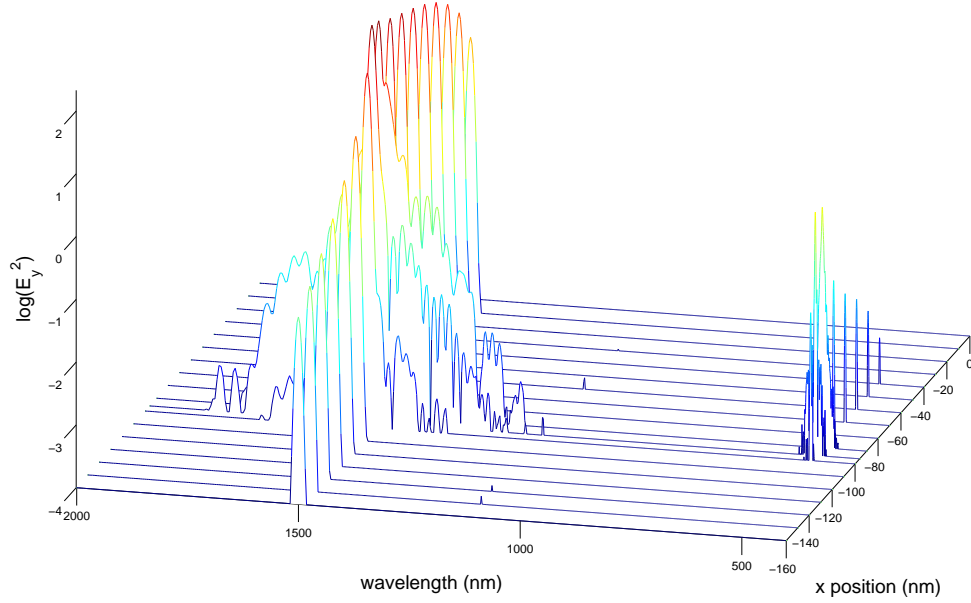
Figure 3.26: $E_y{}^2$ spectrum calculated at different $x$ positions. The source has 300 fs pulse length at 1.5 $\mu m$. $E_y{}^2$ is normalized with respect to the source peak intensity.

Regarding the results for 300 fs incident pulse length, shown in figures 3.25 and 3.26, we firstly observe higher peak intensities in the $E_x{}^2$ and $E_y{}^2$ spectrum due to longer excitation. Hence, the third harmonic at 500 nm is more prominent. Since longer pulse length narrows the bandwidth of the incident electric field, the antenna resonance becomes sharper with a higher peak intensity. This effect is comparatively shown in figure 3.27.

It should be noted that none of the nonlinear effects are observed without the resonant nanoantenna albeit same pulses of peak amplitude $1e8$ V/m are employed. As a result, we show that near field of the resonant nanoantenna can be used for lowering the required large incident electric field for nonlinear interactions. Furthermore, the resonant nanoantenna provides position dependent and polarized nonlinear generations.

Figure 3.27: $E_x{}^2$ spectrum calculated at the top left corner ($x = -95$ nm, $y = 25$ nm) of the resonant stripe nanoantenna is compared for 150 fs and 300 fs source pulse lengths at 1.5 $\mu m$. $E_x{}^2$ and $E_x{}^2$ of the source are normalized with respect to the source peak intensities of corresponding pulse lengths.

# Chapter 4

# FABRICATION

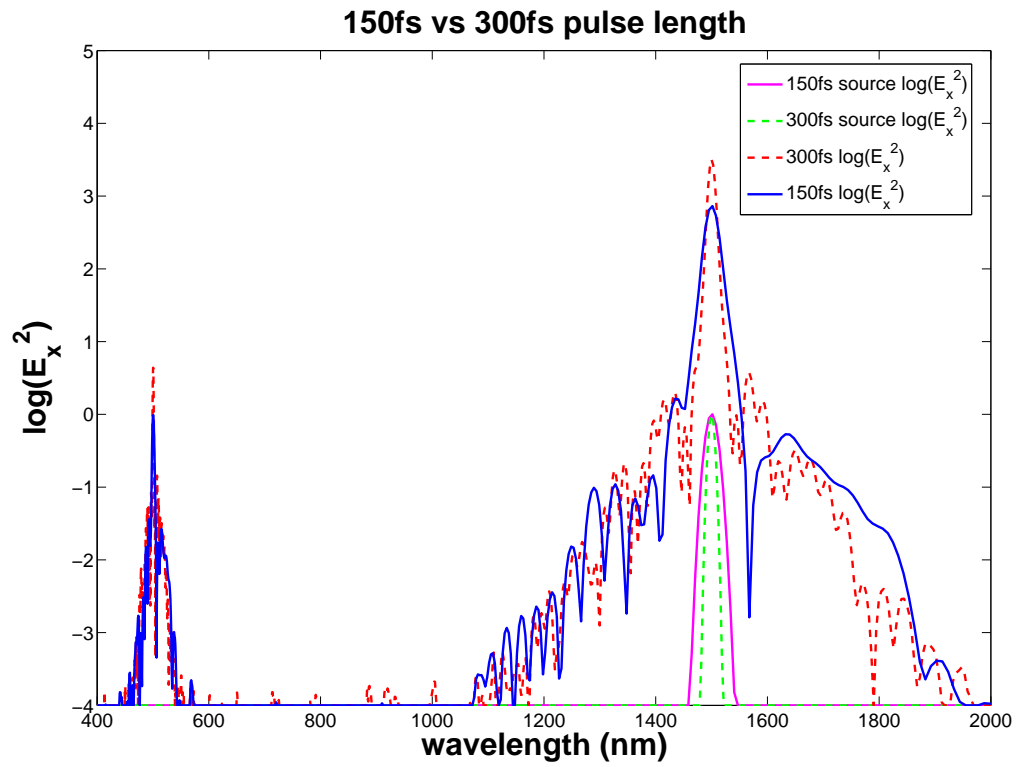In this chapter, our effort for fabrication of gold nanoantennas is presented. Here we provide scanning electron microscope (SEM) images of gold nanoantennas defined on several substrates and investigate the effect of substrate dependence on nano fabrication.

Today nano structures can be defined by either electron beam lithography, focused ion beam (FIB) milling or nano imprint lithography [30]. Of the three methods, we exploit FIB milling due to its versatility. FIB milling is the fastest way of nano scale prototyping. It does not require any resist spread, lift-off or etching. Milling is achieved via accelerated Ga ions; therefore, ion beam parameters such as current, voltage and dwell time should be optimized for the specific milling process.

Here the results obtained with FEI's Nova 600 NanoLab DualBeam system are demonstrated. We first provide SEM images of gold nanoantennas fabricated on $As_2Se_3$ (arsenic selenide). Figure 4.1 presents the fabrication setup. We begin fabrication procedure with evaporating about 1 $\mu m$ of $As_2Se_3$ thin film on appropriately cleaned glass substrate. On top of $As_2Se_3$, 50 nm of gold is deposited by thermal evaporation. Finally, FIB milling of gold is performed where
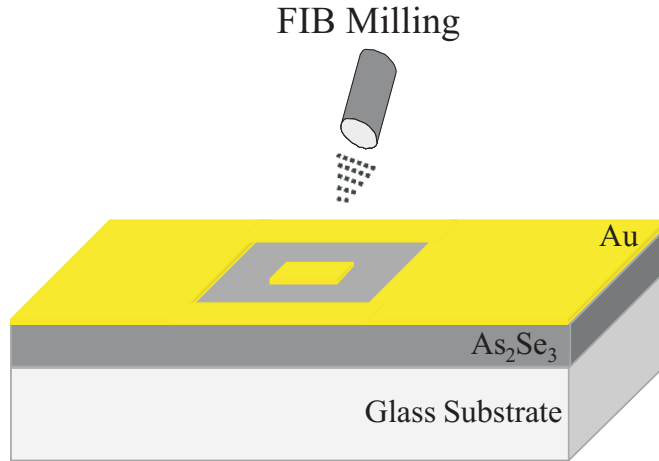
Figure 4.1: Gold nanoantenna fabrication on $As_2Se_3$ evaporated glass substrate.

optimized ion beam parameters are specified experimentally. As a result, stripe nanoantennas at the fundamental resonance ($\lambda = 1.5$ $\mu m$ incident radiation) on $As_2Se_3$ are realized. The antenna array is shown in figure 4.2.

The same gold nanoantenna array is defined on bare glass substrate for comparison. Figure 4.3 shows that gold nano stripes on glass have better shapes albeit they are not perfect. This difference can be attributed to the softness of $As_2Se_3$. While milling gold selectively, high energy Ga ions sputter and pass through the soft $As_2Se_3$ material causing unintentional and random milling. Since lower energy Ga ions require longer dwell times for gold milling, thereby increasing inadvertent gold removal, lower accelerating voltage and beam current is not a solution. High resolution FIB milling of the interface between hard and soft materials is problematic.

Furthermore, the SEM images in figures 4.2 and 4.3 are blurred due to charging caused by the insulating $As_2Se_3$ and glass substrates. Charging is the worst effect experienced in FIB milling and electron beam lithography which prevents high resolution fabrication and imaging. This can be overcome with low vacuum operation albeit it is not appropriate for high resolution milling and imaging. Another way of eliminating the charging effect is gas assisted milling which ensures more accurate milling of specific insulating materials.
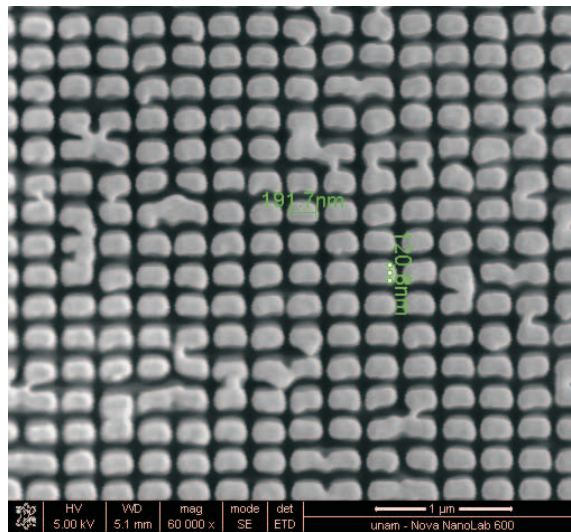
Figure 4.2: Gold stripe nanoantennas on $As_2Se_3$.
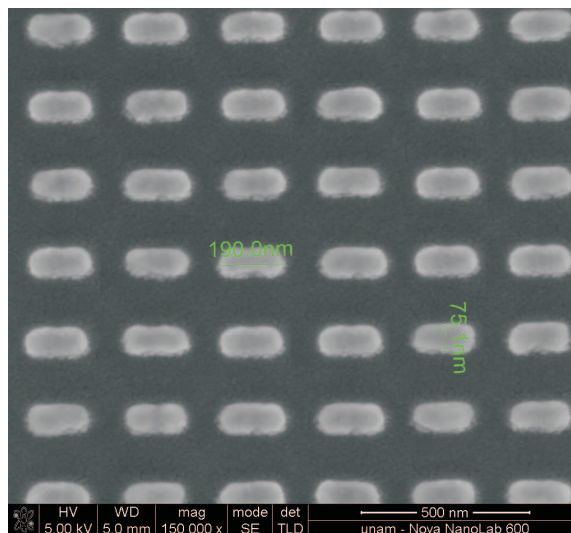


Figure 4.3: Gold stripe nanoantennas on glass.
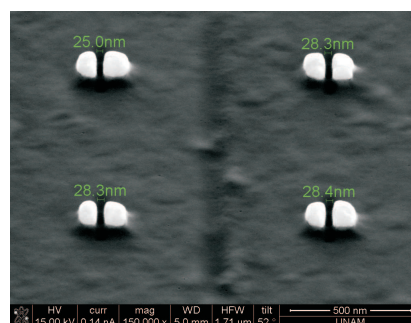


Figure 4.4: Gold stripe nanoantennas on silicon.

Since silicon is both semiconducting and a relatively hard material, gold thin film on silicon substrate allows high resolution definition of gold nanoantennas as seen in figure 4.4. However, low roughness and sharply defined structures should be achieved on all substrates, since near fields associated with imperfections can be detrimental for resonance.

Consequently, fabrication of nanoantennas with FIB milling is fast yet substrate dependent. Soft materials cause more ion beam sputtering thereby undesirable random milling. Since nanoantennas show near field enhancement for a band of antenna lengths, accurate definition of antenna shape is crucial.

# Chapter 5

# CONCLUSIONS AND FUTURE WORK

In conclusion, we propose that resonance characteristics of optical nanoantennas for a specific incident wavelength is governed by substrate, antenna length along the polarization direction of the incident electric field and the antenna shape. This saves us from the burden of numerous simulations and gives us a starting point. We also claim that we can account for the $E_x{}^2$, $E_y{}^2$ and $E_z{}^2$ components of the resonant nanoantenna radiation by taking into account the electron acceleration due to specific $E$ and $B$ components of the incident optical field. Furthermore, we also employ the near field enhancement of the resonant optical nanoantenna for lowering the required large incident electric field for optical nonlinear generations. This could be very promising in the field of nonlinear optics. Finally, we show that the fabrication of nanoantennas with FIB milling is fast yet substrate dependent.

Our future work will consist of realizing the numerical calculation results with near electric field measurements of the resonant nanoantenna including the nonlinear generations. Thus, obtaining the ability of near electric field measurement

technique, we will be able to try new horizons in the realm of resonant optical nanoantennas.

# Bibliography

[1] P. Muhlschlegel, H. J. Eisler, O. J. F. Martin, B. Hecht, and D. W. Pohl, "Resonant optical antennas," *Science*, vol. 308, pp. 1607–1609, 2005.

[2] P. Ghenuche, S. Cherukulappurath, T. H. Taminiau, N. F. van Hulst, and R. Quidant, "Spectroscopic mode mapping of resonant plasmon nanoantennas," *Physical Review Letters*, vol. 101, pp. 1168051–1168054, 2008.

[3] A. Alu and N. Engheta, "Tuning the scattering response of optical nanoantennas with nanocircuit loads," *Nature Photonics*, vol. 2, pp. 307–310, 2008.

[4] P. Biagioni, J. S. Huang, L. Duo, M. Finazzi, and B. Hecht, "Cross resonant optical antenna," *Physical Review Letters*, vol. 102, pp. 2568011–2568014, 2009.

[5] S. Kim, J. Jin, Y. J. Kim, I. Y. Park, Y. Kim, and S. W. Kim, "High harmonic generation by resonant plasmon field enhancement," *Nature*, vol. 453, pp. 757–760, 2008.

[6] L. Tang, S. E. Kocabas, S. Latif, A. K. Okyay, D. S. L. Gagnon, K. C. Saraswat, and D. A. B. Miller, "Nanometre scale germanium photodetector enhanced by a near-infrared dipole antenna," *Nature Photonics*, vol. 2, pp. 226–229, 2008.

[7] D. K. Kotter, S. D. Novack, W. D. Slafer, and P. Pinhero, "Solar nantenna electromagnetic collectors," *Proceedings of ES2008*, 2008.

[8] G. von Maltzahn, A. A. J. H. Park, N. K. Bandaru, S. K. Das, M. J. Sailor, and S. N. Bhatia, "Computationally guided photothermal tumor therapy using long-circulating gold nanorod antennas," *Cancer Res.*, vol. 69, pp. OF1–OF9, 2009.

[9] E. Cubukcu, N. Yu, E. J. Smythe, L. Diehl, K. B. Crozier, and F. Capasso, "Plasmonic laser antennas and related devices," *IEEE Journal of Selected Topics in Quantum Electronics*, vol. 14, pp. 1448–1461, 2008.

[10] C. A. Balanis, *Antenna Theory*. Wiley, 2005.

[11] M. L. Brongersma, "Engineering optical nanoantennas," *Nature Photonics*, vol. 2, pp. 270–272, 2008.

[12] A. Kinkhabwala, Z. Yu, S. Fan, Y. Avlasevich, K. Müllen, and W. E. Moerner, "Large single molecule fluorescence enhancements produced by a bowtie nanoantenna," *Nature Photonics*, vol. 3, pp. 654–657, 2009.

[13] R. Adatoa, A. A. Yanika, J. J. Amsdenc, D. L. Kaplanc, F. G. Omenettoc, M. K. Honge, S. Erramillib, and H. Altug, "Ultra sensitive vibrational spectroscopy of protein monolayers with plasmonic nanoantenna arrays," *PNAS*, vol. 106, pp. 19227–19232, 2009.

[14] T. H. Taminiau, F. D. Stefani, F. B. Segerink, and N. F. V. Hulst, "Optical antennas direct single molecule emission," *Nature Photonics*, vol. 2, pp. 234–237, 2008.

[15] E. Hehct, *Optics*. Addison Wesley, 1987.

[16] S. J. Orfanidis, *Electromagnetic Waves and Antennas*. 2005.

[17] S. A. Maier, *Plasmonics Fundamentals and Applications*. Springer, 2007.

[18] I. El-Kady, M. M. Sigalas, R. Biswas, K. M. Ho, and C. M. Soukoulis, "Metallic photonic crystals at optical wavelengths," *Physical Review B*, vol. 62, pp. 15299–15302, 2000.

[19] Z. W. Liu, Q. H. Wei, and X. Zhang, "Surface plasmon interference nano-lithography," *Nano Letters*, vol. 5, pp. 957–961, 2005.

[20] M. S. Rill, C. E. Kriegler, M. Thiel, G. von Freymann, S. Linden, and M. Wegener, "Negative index bianisotropic photonic metamaterial fabricated by direct laser writing and silver shadow evaporation," *Optics Letters*, pp. 19–21, 2009.

[21] S. Linden, C. Enkrich, M. Wegener, J. Zhou, T. Koschny, and C. M. Soukoulis, "Magnetic response of metamaterials at 100 terahertz," *Science*, vol. 306, pp. 1351–1353, 2004.

[22] E. Ozbay, "Plasmonics: Merging photonics and electronics at nanoscale dimensions," *Science*, vol. 311, pp. 189–193, 2006.

[23] L. Novotny, "Optical antennas tuned to pitch," *Nature*, vol. 456, p. 887, 2008.

[24] M. Schnell1, A. Garcia-Etxarri, A. J. Huber, K. Crozier, J. Aizpurua, and R. Hillenbrand, "Controlling the near field oscillations of loaded plasmonic nanoantennas," *Nature Photonics*, vol. 46, pp. 1–5, 2009.

[25] E. S. Barnard, J. S. White, A. Chandran, and M. L. Brongersma, "Spectral properties of plasmonic resonator antennas," *Optics Express*, vol. 16, pp. 16529–16537, 2008.

[26] E. Cubukcu, E. A. Kort, K. B. Crozier, and F. Capasso, "Plasmonic laser antenna," *Applied Physics Letters*, vol. 89, pp. 0931201–0931203, 2006.

[27] J. A. Schuller, E. S. Barnard, W. Cai, Y. C. Jun, J. S. White, and M. L. Brongersma, "Plasmonics for extreme light concentration and manipulation," *Nature Materials*, vol. 9, pp. 193–204, 2010.

[28] W. L. Barnes, A. Dereux, and T. W. Ebbesen, "Surface plasmon subwavelength optics," *Nature*, vol. 424, pp. 824–830, 2003.

[29] J. K. Kim, "Investigation of high nonlinearity glass fibers for potential applications on ultrafast nonlinear fiber devices," *PhD. Thesis*, 2005.

[30] B. Bhushan, *Springer Handbook of Nanotechnology.* Springer, 2004.